PROCESS CONTROL STRATEGIES IN ADDITIVE MANUFACTURING

By

RINKAL KISHORKUMAR DESAI

A thesis submitted to the

School of Graduate Studies

Rutgers, The State University of New Jersey

In partial fulfillment of the requirements

For the degree of

Master of Science

Graduate Program in Industrial and Systems Engineering

Written under the direction of

Dr. Tuğrul Özel

And approved by

_____

_____

_____

_____

New Brunswick, New Jersey

May 2019

ABSTRACT OF THE THESIS

PROCESS CONTROL STRATEGIES IN ADDITIVE MANUFACTURING

by RINKAL KISHORKUMAR DESAI

Thesis Director:

Dr. Tuğrul Özel

Additive manufacturing (or 3D-printing) processes such as fused filament fabrication of polymer constructs and laser based sintering and fusion of metal powder which can produce nearly fully dense parts with complex geometry by following layer-to-layer scanning strategies on feedstock material with pre-specified layer thickness find many applications in industry ranging from prototype fabrication to actual parts and components production.

In this thesis, we study the control schemes that can be developed in improving the extruded polymer consistency in form and temperature, and fused track quality in laser-based melting and fusion by using observable process variables and applying control on controllable variables. Specifically, system identification methods are used to obtain transfer function for Liquefier block in a fused filament fusion systems and simulations are

conducted to introduce a suitable control strategy. The control strategy simulations for temperature control of Liquefier block takes in accounts the load to the system (filament feed rate) and a suitable feedback compensator is designed. The Lead-lead feedback compensator has proved to provide faster settling time and negligible steady state error. Also, an XY positioning system is considered for studying the trajectory control using feedback and iterative learning control schemes. The iterative learning control method is found to be very effective in reducing contour error during tracking of trajectories with sharp corners. The results obtained from these studies are expected to provide more information about the additive manufacturing process control which can be used for further validation of modelling studies or for industrial purposes.

TABLE OF CONTENTS

LIST OF TABLES

CHAPTER 2

CHAPTER 4

CHAPTER 5

LIST OF FIGURES

CHAPTER 1

CHAPTER 2

CHAPTER 4

CHAPTER 5

Chapter 1

INTRODUCTION

Additive manufacturing (or 3D-printing) processes such as fused filament fabrication of polymer constructs and laser-based sintering and fusion which can produce nearly fully dense parts with complex geometry by following layer-to-layer scanning strategies on feedstock material with pre-specified layer thickness find many applications in industry ranging from prototype fabrication to actual parts and components production.

Some of the examples of the additive manufacturing processes and their working principles are shown in Fig 1.1. In the fused filament fabrication process, the filament is fed into the heated extruder by two electric motor controlled pinch rollers. The filament is heated up to its melting point which is monitored by a temperature sensor (thermocouple or thermistor). The printing process starts after the extrusion chamber reaches the desired temperature, which is later maintained by regulating the current supplied to the heater's coils. The filament solidifies on leaving the nozzle, and laid on the table to print the desired shape. The positioning table is controlled by computer signals to build the object layer by layer from the "Standard Triangle Language" (STL) or other file format file.

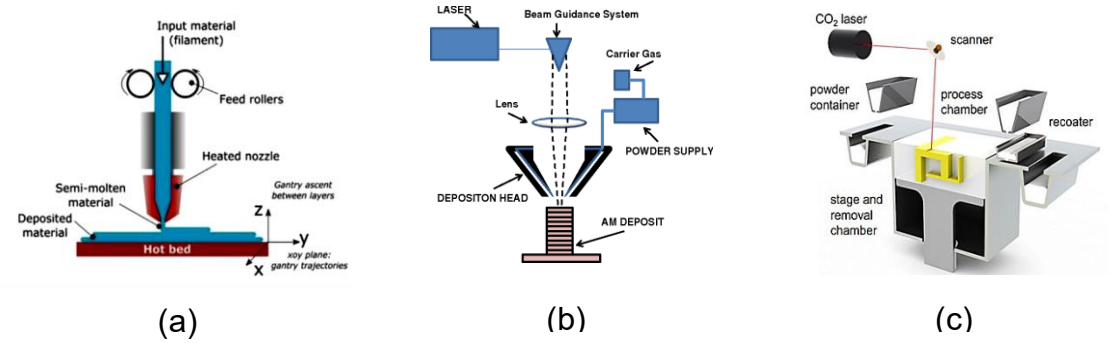

Figure 1. 1: (a) Fused filament fabrication (FFF) [Turner et al. 2014], (b) Laser metal deposition (LMD) [William F. 2014], (c) Laser powder bed fusion (L-PBF) [Source: sculpteo.com].

The Laser metal deposition (LMD) (Fig. 1.1.(a)), which is Directed Energy Deposition (DED) system, uses a similar process where the energy source is either laser beam or electron beam. The feedstock material can either be a fine powder or wire (filament). The laser scan head are of different architecture depending on the manufacturer, it follows the design file and moves accordingly. This process is beneficial to repair aging parts such as metal parts used in military aircraft, ceramic dentures, etc. When laser is used as an energy source and feedstock material is in powder form usually a shielding gas such as Argon or Nitrogen is used.

1.1 Applications of Additive manufacturing

Materials such as bones, muscles, wood, etc. are not only difficult to manufacture but quite impossible to manufacture with subtractive manufacturing. Additive manufacturing seems promising to develop such intricate structures while producing an end product of desired shape and size. The Additive manufacturing uses less resources in terms of material as well

as labor. As seen in Fig. 1.1 “Additive manufacturing” generates lesser waste than “Subtractive manufacturing” as it is developed layer-by-layer and not carved out of a large metal workpiece. The applications of additive manufacturing are in medical devices (prosthetics, artificial joints, etc.), automotive and aerospace parts, architectural artifacts, fine jewelry, processed food industry and many other fields.

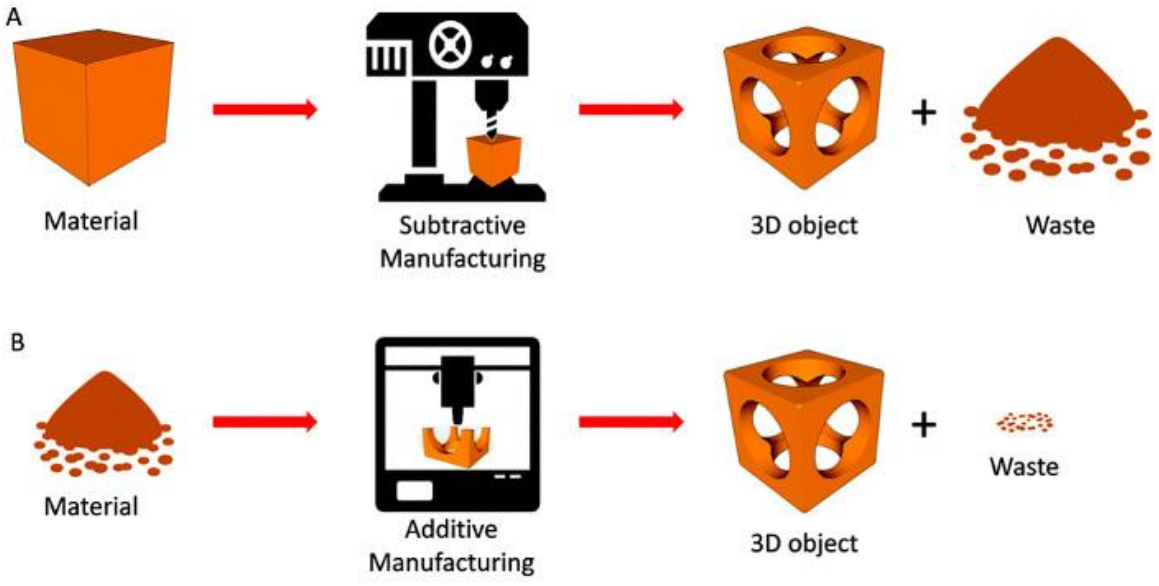

Figure 1. 2: Comparison between (a) additive manufacturing and (b) subtractive manufacturing [source: https://www.3dnatives.com/en/3d-printing-vs-cnc-160320184/]

Automotive and Aerospace Components: Automotive and aerospace industries look for a technology that consumes less time and money. In sectors such as aerospace, where material cost is high even for a small quantity, AM technology is providing a new way to offer cheaper solution by optimizing the resources significantly over conventional manufacturing (see Fig. 1.2). There a number of additively fabricated parts and components

in modern automobiles and aircrafts. For example, a jet engine prototype (see Fig. 1.3) was constructed using a laser powder bed fusion (L-PBF) based AM technology.

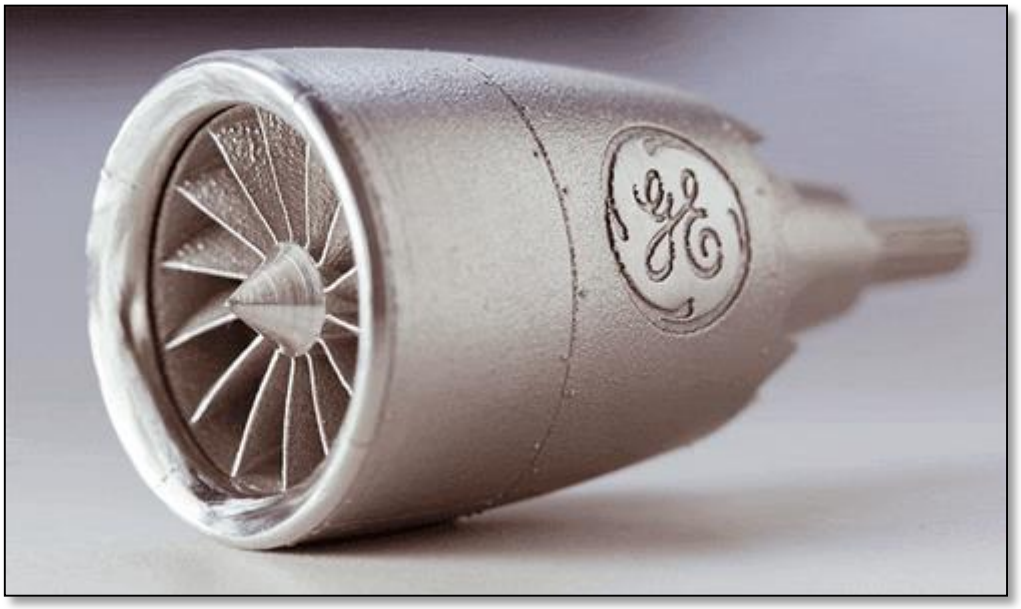

Figure 1. 3: A miniature jet engine [source:ge.com]

Miniature air vehicles and satellites are being developed and deployed for stealth operation and intelligence gathering to improve mission effectiveness. These vehicles are equipped with micro turbines.

Medical Devices: Surgical equipment's and implants are clusters of medical devices that utilized miniature components and systems. The minimally invasive surgery is developed to reduce the pain and speed up the recovery time of the patients. Various equipment such as miniaturized video cameras, micro holes for fiber optic cables and surgical equipment are necessary to successfully carry out the surgery. Various sizes of implants ranging from meso-to-micro such as of the spinal cord are used to stabilize the bone after an injury (see

Fig. 1.4). These implants use the minimally invasive surgery methods to reduce the healing time.

Figure 1. 4: 3D printed spinal cord implant approved by FDA [source: K2M]

Another group of medical devices is *orthopedic implants* as shown in Fig.1.5. Orthopedic implants are devices that replace a fractured bone or missing joint using pins, screws, plates and rods fabricated of metals, ceramics or alloys. The implants cannot be of standard shape and size just like dentures which makes 3D printing more relevant technology to fabricate it.

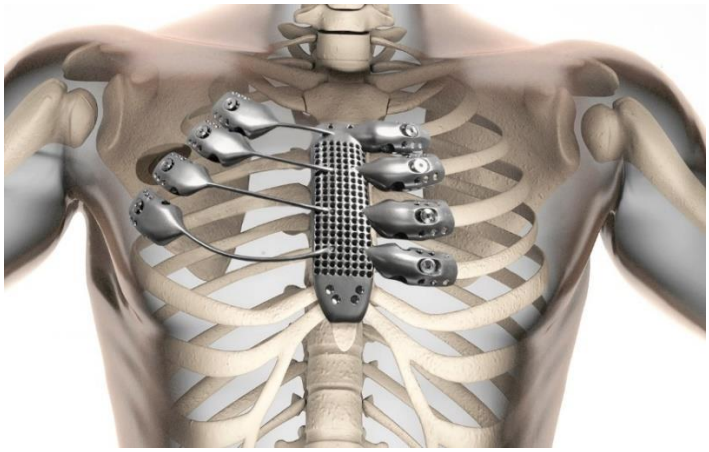

Figure 1. 5: Rib cage implants [Source: Anatomics/CSIRO]

1.2 Process Monitoring and Control Strategies

As much as a robust system is desirable it is a challenging process. A common approach involves process monitoring of the known and/ or critical parameters of a system and maintaining them at desired states. A complex system is usually divided in modules/subsystems which individually has its own input variables (controlled variables), input parameters (typically constant), desired outputs (set points) and disturbances (noise etc.). Each module has different system parameters which are either controllable or observable, which help us classify between parameters that can be controlled or just monitored. System lags, delays, dead zones, etc. should be accounted in design to achieve a finer control. The controllers along with filters are proven to stabilize a lot of systems but they too introduce their own time delay. A feedback control, a feedforward control (known uncertainties), an iterative or repetitive control (when the past behavior is known), a Fuzzy inference system (linguistic variables), etc. are type of control methods which can be used to create a hybrid system.

1.3 Rationale and Motivation

AM is very promising manufacturing field with myriad of applications but there are limitations as it is still a developing technology. To achieve more precise and higher quality end-products the systems and processes need to be built smarter, more robust and predictable. For a more responsive process which is resilient to uncertainties, an intelligent process control model is indispensable.

It is the premise of this proposed work that only experimental and modeling studies will help in gaining a fundamental understanding of the control strategies. The better understanding will help additive manufacturing engineers to select the process parameters such as energy density, feed stock material flow rate, scan speed or filament feeding speed to improve the productivity and obtain good construct quality in additively fabricated parts and components.

1.4 Research Objectives

The objective of this research is to investigate the additive manufacturing processes such as Fused Filament Fabrication (FFF), Laser Powder Bed Fusion (L-PBF) and Laser Metal Deposition (LMD) with a control theory perspective and provide a stability analysis of the system.

Another objective of this study is to investigate the impact of designing a controller to control and manipulate system parameters such as feedstock rate (in LMD), extruded filament temperature (in FFF), extruded filament trajectory (in FFF), energy density and melt pool controls (in L-PBF or in LMD) to strengthen the robustness of additive manufacturing processes.

The third objective of this study is to implement a feedback control strategy in order to monitor and control the extruded filament size and temperature in FFF based additive manufacturing processes.

The fourth objective of this study is to investigate control strategies implementable for L-PBF or LMD based metal additive manufacturing processes. Specifically process control

aspects will be investigated for powder feedstock delivery and control, laser power, scan speed and energy density control, as well as monitoring and controlling the condition of the melt pool for process anomalies will be performed.

Chapter 2

PROCESS CONTROL IN FUSED FILAMENT FABRICATION PROCESS

2.1 Fused Filament Fabrication

Additive manufacturing is one of the most important drivers of innovation in manufacturing industries. Melt extrusion based additive manufacturing processes such as fused filament fabrication is widely used. FFF consists of pushing a filament of thermoplastic (e.g. Acrylonitrile-Butadiene Styrene (ABS), polylactic acid (PLA), polystyrene (PS), polyamides (nylon)) through a liquefier and depositing the semi-molten extruded thin filament onto the support surface.

The key elements of melt extrusion are material feed mechanism, liquefier, print nozzle, build surface and environment. The working of FFF process and the components of the liquefier are shown in Fig. 2.1.

In these systems, the liquefier is a metal block with a hole machined for the filament to flow through. Filament refers to the total length of extrudate used to manufacture the part. Filament segment is the length of filament that is deposited by the machine nozzle in one horizontal plan before reversing the deposition direction. A gantry moves the print nozzle in the horizontal x–y plane as the material is deposited on a build surface that can be moved in the vertical z direction. Build surface is a surface on which the melted extrudate is deposited layer upon layer. The main inputs to this system are heater coil temperature, feedstock rate, fan speed and the path of the extruder. The feedstock material affects the

amount of heat loss in the heat block as well as the re-solidification of the extruded feedstock.

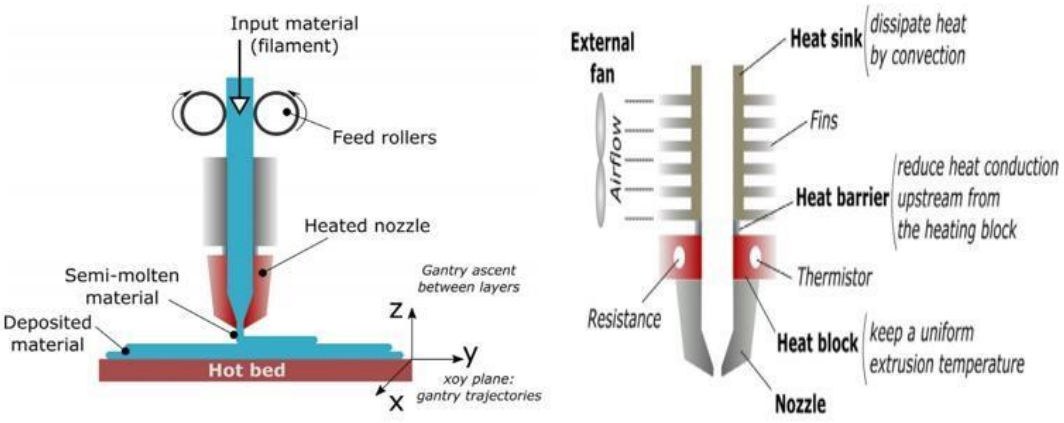

(a) Overall system view (b) Cross sectional view

Figure 2.1: A typical Fused Filament Fabrication system [Turner et al. 2014].

To determine the stability of the process or further control it and make It faster and accurate a system model needs to be created. This kind of analysis typically helps in designing a controller for a system so that it works efficiently and shows reproducibility.

2.2 Process Parameters and Variables

The FFF system has three subsystems; (i) liquefier, (ii) filament driving system, and (iii) positioning system. Three different subsystems are separately studied to build a system model. All three system uses different analogy to compute their respective transfer functions. The filament drive mechanism uses stepper motors and pinch rollers (gear box) to function and hence are analogous to electromechanical system. For liquefier modelling a system identification approach is used as it is a unique system and difficult to model. The

positioning system has two kind of mechanism involved i.e. lead screw and conveyor belt mechanism. Modelling them as transfer functions will give us how well the model works and comment on their stability.

In an FFF process a three-axis position control system is used. We can either control its position or velocity (we need to check if the velocity is constant or variable). Another important input component is extruder and liquefier. Also, the filament structural properties affect the process. In the liquefier there is a cooling system and then a thermistor to heat the filament. The heat sink is to reduce heat conduction into the filament in the upper region so it stays sturdier. The thermistor liquefies the filament and the extruder streamlines the flow of liquid filament. So, the filament has different thickness when it entered the heat sink, when it is liquefied and when it leaves the extruder. Apart from thickness they have different temperatures and cooling rates. So now we will define the input parameters (designed output parameters) and a basic block diagram can be formulated as given in Fig. 2.2. Where, T_{fn} is the temperature of the filament at different states for n= 0,1,3,.. ; T_{fex} is the extruded filament temperature; D_{fn} is the diameter of filament at different states; and D_{fex} is the extruded filament diameter.

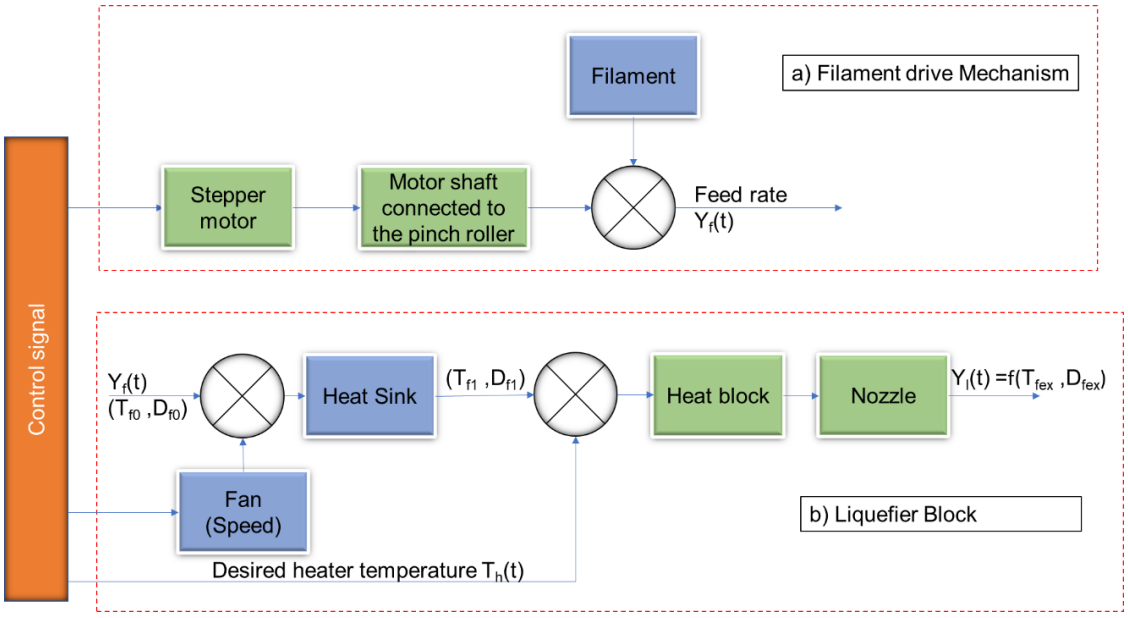

Figure 2. 2: Basic block diagram of a filament drive mechanism and a liquefier section of the Fused Filament Fabrication system.

2.3 Filament Drive Mechanism

The filament is connected to a stepper motor which pushes it further to the gear system. The pinch rollers which aid in driving the filament are a set of gears. Ricardo (2014) modelled a hybrid stepper motor with 2 phases and 3 teeth has a phase resistance R_w, phase inductance L_w, phase current $i_j(t)$, phase terminal voltage $u_j(t)$ and back emf e_j (t) (j = A , B) two phases of motor. Applying Kirchhoff's voltage law for the loop he gave electrical input equation,

$$L_w \frac{di_j(t)}{dt} = -R_w i_j(t) - e_j(t) + u_j(t) \qquad (2.1)$$

The back emf is given by below equations. K_m is motor constant, p the number of motor pole pairs, ω_m is the rotor angular speed θ_m ;

$e_A\,(\mathrm{t}) = -\mathrm{K}_m\,\omega_m \sin(\mathrm{p}\theta_m);$ $\qquad e_B\,(\mathrm{t}) = -\mathrm{K}_m\,\omega_m \cos(\mathrm{p}\theta_m);$

Applying Laplace transformation to Equation (2.1) above gives

$$\mathrm{U}_j\,(\mathrm{s}) = \mathrm{Z}_{mot}\,\mathrm{I}_j\,(\mathrm{s}) + \mathrm{E}_j\,(\mathrm{s}) \tag{2.2}$$

The output of stepper motor is an angular displacement. The mechanical torque is obtained as result of electromagnetic force produced in the stepper motor. The energy balance equation for stepper motor is gives in Equation (2.3) below,

$$\mathrm{J}\frac{\mathrm{d}\omega_m}{\mathrm{dt}} = \tau_{em} - \mathrm{B}\omega_m - \tau_{dm} - \tau_l \tag{2.3}$$

Where $\tau_{em} = \mathrm{K}_m\left(-i_{mot_A}\sin(\mathrm{p}\theta_m) + i_{mot_B}\cos(\mathrm{p}\theta_m)\right)$is the motor's electromagnetic torque, *J* its moment of inertia, *B* the viscous friction coefficient, $\tau_{dm} = T_{dm}\sin(2\mathrm{p}\theta_m + \varphi)$ is the detent torque, T_{dm} the detent torque amplitude, a phase shift associated with τ_{dm} and τ_l the external load torque. ($\varphi = \tau_{em} - \mathrm{B}\omega_m - \tau_{dm} - \tau_l$)

The Laplace transform of Equation (2.3) above is given as,

$$\omega_m(s) = \frac{\tau_{em}(\mathrm{s}) - \tau_{dm}(s) - \tau_l(\mathrm{s})}{sJ+B} \tag{2.4}$$

Combining the Equation (2.2) and Equation (2.3) we get the transfer function filament drive mechanism as below,

$$\frac{\omega_m(s)}{U_j(s)} = \frac{\tau_{em}(\mathrm{s}) - \tau_{dm}(s) - \tau_l(\mathrm{s})}{\left(Z_{mot}\,I_j(s) + E_j(s)\right)(sJ+B)} \tag{2.5}$$

The transfer function of the filament drive is a first order equation and can be compared to first order system. This is an open loop system and hence lacks in process control.

2.4 Positioning System

This system is responsible for following the design file. It aims to be on the same coordinate as in the design file. The three axis are differently operated with three different stepper motors (see Figure 2.3). The stepper motor rotor is connected to either a belt driven system or a lead screw. Another parameter that will affect the system or create an offset is the angle between all the axis. But that can be avoided by frequent calibration of the positioning system.

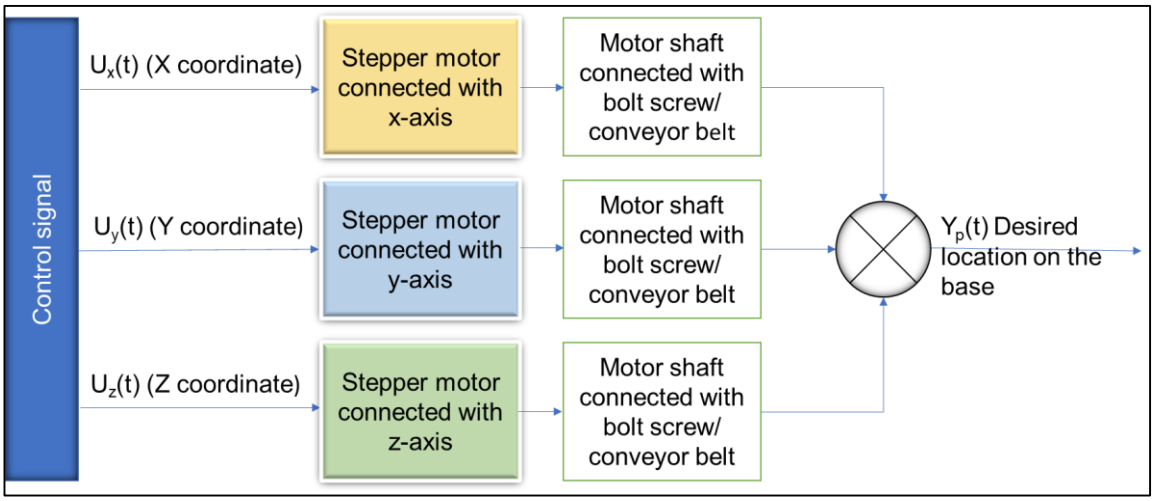

Figure 2. 3: Block diagram for the positioning system**.**

2.5 Liquifier Thermal System

The most influential system of an FFF process is liquefier. The liquefier has a heat sink, heat barrier, heat block and nozzle, each having a different temperature at a given time. There are two ways to model this system, based on thermal equations or from thermal finite element analysis.

As reported by Shah et al. (2018), the thermal modeling of a liquefier involves a heat sink, a heat barrier, a heat block and a nozzle. The different parts of the liquefier exhibit different types of heat transfer. Considering from the top, heat sink involves convection type heat transfer phenomenon. Heat sink is constructed with fins which enhance the cooling process. Also, a fan is attached to increase the heat transfer by blowing air. This can be given by Newton's Law of cooling as follows,

$$T(t) = T_s + (T_o - T_s)e^{(-ct)} \tag{2.6}$$

where, T(t) is the temperature of an object at a certain time (K), *t* is time (s), T_s is the temperature of the surroundings at the time (K), *c* is a cooling constant which depends on the fan velocity (1/s).

The temperature obtained in the heat sink region is due to the generation of heat in the heat block. There is a titanium made heat barrier in between the sink and the heat block which partially insulates the heat sink. So only fraction of heat is passed to the sink as the heat barrier slows down conduction due to its low thermal conductivity. Which can be given as below,

$$T_o = l\,T_1 \tag{2.7}$$

where T_0 is the initial temperature of the object attained from heat block due to partial conduction (Kelvin, K), *l* is the fraction of heat passed through the heat barrier, *c* is the cooling constant which depends on the fan velocity (1/s).

The heat block uses a thermistor which generates heat in accordance to the electrical energy(current) given to it. The heat block uses the conduction principle to melt the filament. The heat conduction follows as the Equation 2.8,

$$\boldsymbol{q = k\,A\,\frac{u(t,x) - u(t,x+\Delta x)}{\Delta x}} \tag{2.8}$$

All the above equations (Eqs. 2.6, 2.7 and 2.8) when placed in the equation of heat conservation it is very difficult to attain a transfer function solution analytically. So we will use a different approach, to determine the transfer function of the liquefier. Finite element analysis of liquefier gives the temperature profile with respect to time which can be used to compute transfer function using a system identification method available in MATLAB software.

2.6 System Identification Approach

System identification is applied by using MATLAB in which sampled data is used to estimate a transfer function of that system is obtained. Data extracted from thermal analysis (Shah et al. 2018) was stored as Excel spreadsheet, and then imported to the MATLAB workspace. The data from the 9-point evaluated temperature profile will then be processed in MATLAB. Using the system identification toolbox we will compute a transfer function, which we will be used for further processes. The data set has temperature for 5 points in the heat sink, bottom of the heat sink, top of the heat block and bottom of the heat block. Using the transfer function estimation model, eight transfer functions were found. The TF_1 corresponds with system input as heater temperature and output as steel top temperature. Similarly, it can be seen in the Table 2.1 below the inputs and outputs of all the transfer functions. The subscript of transfer function denotes the fan speed.

Table 2.1 Case 'a' – Liquefier block transfer function (Heat sink fin shape is hexagon and Fan Speed = 0 m/s)

Input to output		**Transfer function obtained with System Identification**	**% Fit to data**	**MSE**
Heater to steel top	$Tf1_0$	$\frac{0.01249}{s^2 + 0.2758\,s + 0.01285}$	99.51%	0.01541
Steel top to sink bottom	$Tf2_0$	$\frac{0.01701\,s + 0.001503}{s + 0.006693}$	99.49%	0.000976
Sink bottom to Sink1	$Tf3_0$	$\frac{s + 2.778e09}{s + 2.789e09}$	99.61%	0.0005531
Sink1 to Sink2	$Tf4_0$	$\frac{s + 3.999e08}{s + 4.011e08}$	99.67%	0.0004065
Sink2 to Sink3	$Tf5_0$	$\frac{s + 4.093e07}{s + 4.102e07}$	99.7%	0.0003244
Sink3 to Sink4	$Tf6_0$	$\frac{s + 1.043e07}{s + 1.045e07}$	99.73%	0.000278
Sink4 to Sink5	$Tf7_0$	$\frac{s + 3.253e10}{s + 3.26e10}$	99.63%	0.0004958
Sink5 to sink top	$Tf8_0$	$\frac{0.9994\,s + 1.277e13}{s + 1.281e13}$	99.52%	0.0008509

Table 2.2 Case 'b', Liquefier block transfer function (Heat sink fin shape is hexagon and Fan Speed = 10 m/s)

Input to output		**Transfer function obtained with System Identification**	**% Fit to data**	**MSE**
Heater to steel top	$Tf1_{10}$	$\frac{0.01229}{s^2 + 0.2717\,s + 0.01265}$	99.69%	0.006199
Steel top to sink bottom	$Tf2_{10}$	$\frac{0.02395\,s + 0.001775}{s + 0.009249}$	99.01%	0.001709
Sink bottom to Sink1	$Tf3_{10}$	$\frac{0.9959\,s + 1.294e05}{s + 1.299e05}$	99.53%	0.0003784
Sink1 to Sink2	$Tf4_{10}$	$\frac{0.9971\,s + 2.239e05}{s + 2.246e05}$	99.6%	0.0002799
Sink2 to Sink3	$Tf5_{10}$	$\frac{0.9976\,s + 1.082e05}{s + 1.085e05}$	99.64%	0.0002269
Sink3 to Sink4	$Tf6_{10}$	$\frac{0.998\,s + 1.133e05}{s + 1.135e05}$	99.65%	0.0002061
Sink4 to Sink5	$Tf7_{10}$	$\frac{s + 2.303e09}{s + 2.308e09}$	99.58%	0.0003016
Sink5 to sink top	$Tf8_{10}$	$\frac{s + 2.982e13}{s + 2.994e13}$	99.45%	0.0005184

Table 2.3 Case 'c' - Liquefier block transfer function (Heat sink fin shape is hexagon and Fan Speed = 15 m/s)

Input to output		**Transfer function obtained wit System Identification**	**% Fit to data**	**MSE**
Heater to steel top	$Tf1_{15}$	$\frac{0.0169}{s^2 + 0.353\,s + 0.0174}$	99.88%	0.001627
Steel top to sink bottom	$Tf2_{15}$	$\frac{9.32e-07}{s^3 + 0.023\,s^2 + 0.0005837\,s + 5.364e-06}$	99.01%	0.001057
Sink bottom to Sink1	$Tf3_{15}$	$\frac{0.9954\,s + 0.07327}{s + 0.07364}$	99.63%	0.0001501
Sink1 to Sink2	$Tf4_{15}$	$\frac{0.9967\,s + 0.06785}{s + 0.06808}$	99.67%	0.0001124
Sink2 to Sink3	$Tf5_{15}$	$\frac{0.9973s+0.0637}{s + 0.06389}$	99.7%	9.271e-05
Sink3 to Sink4	$Tf6_{15}$	$\frac{0.9977s + 0.0628}{s + 0.06296}$	99.71%	8.594e-05
Sink4 to Sink5	$Tf7_{15}$	$\frac{0.9975\,s + 3.831}{s + 3.841}$	99.56%	0.0002016
Sink5 to sink top	$Tf8_{15}$	$\frac{0.9964\,s + 0.1033}{s + 0.1037}$	99.42%	0.0003498

2.7 Results and Discussion

To understand the overall system dynamics, first let us discuss the filament drive mechanism and liquefier block together. The filament is the "known load" to the heat block of the liquefier. As seen in the figure the heat sink of the liquefier block is attached with a fan operated at a constant speed. The filament is fed into the liquefier using a combination of pinch rollers with a constant speed stepper motor, suggesting that the load will remain constant in operating condition. We will consider three cases, case 'a' has a fan speed 0 m/s, case 'b' has a fan speed 10 m/s and case 'c' has a fan speed 15 m/s . Similarly, three cases use their respective transfer function.

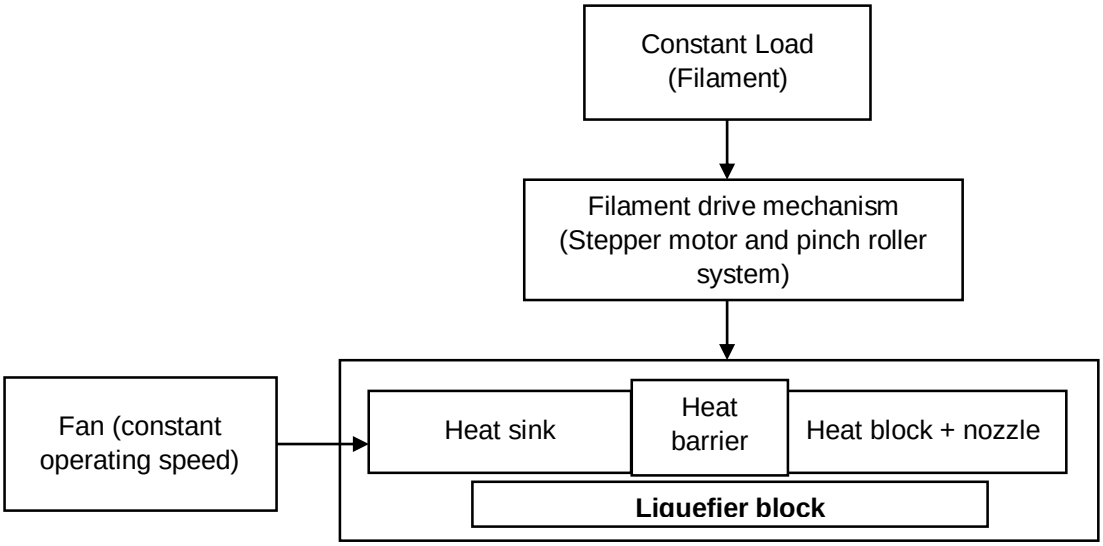

Figure 2. 4: Block diagram for liquefier and filament drive mechanism.

The transfer function obtained in Tables 2.1, 2.2, 2.3 are for no load condition at different fan speeds. Assuming the load (feedstock rate) is constant we can say that it will only change the constant of the transfer function and not the order of the system. Root locus analysis determines a tolerable range for change in load where system stays stable. Transfer

functions associated with heat sink (TF_3 to TF_8) have a pair of pole and zero which is closely located to each other (Fig. 2.7, 2.8, 2.9). Also, pole-zero pairs are located on the x-axis far away from the origin on the left half plane. This can be seen in the RL obtained in MATLAB for the individual transfer function in Fig. 2.7, 2.8, 2.9). The transfer functions of critical importance are TF_1 and TF_2 as they represent the system close to the heater. They are more responsive than others.

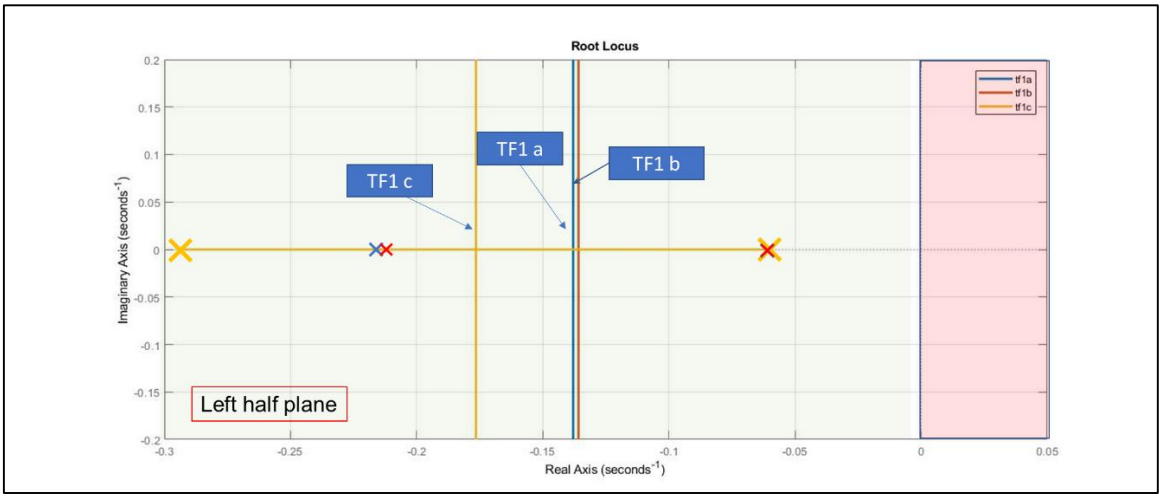

Figure 2. 5: Root locus of TF1 for case 'a', case 'b', and case 'c'.

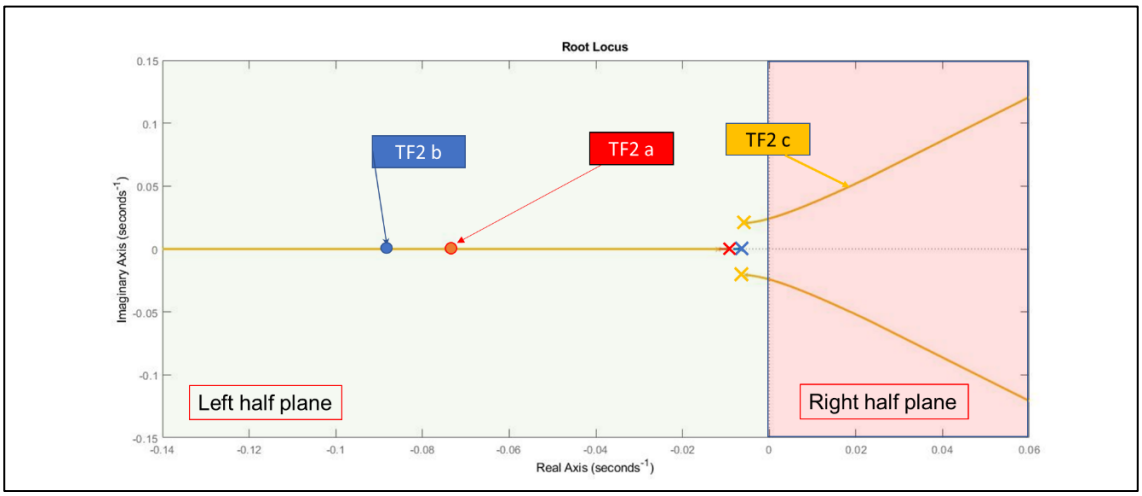

Figure 2. 6: Root locus of TF2 for case 'a', case 'b', and case 'c'.

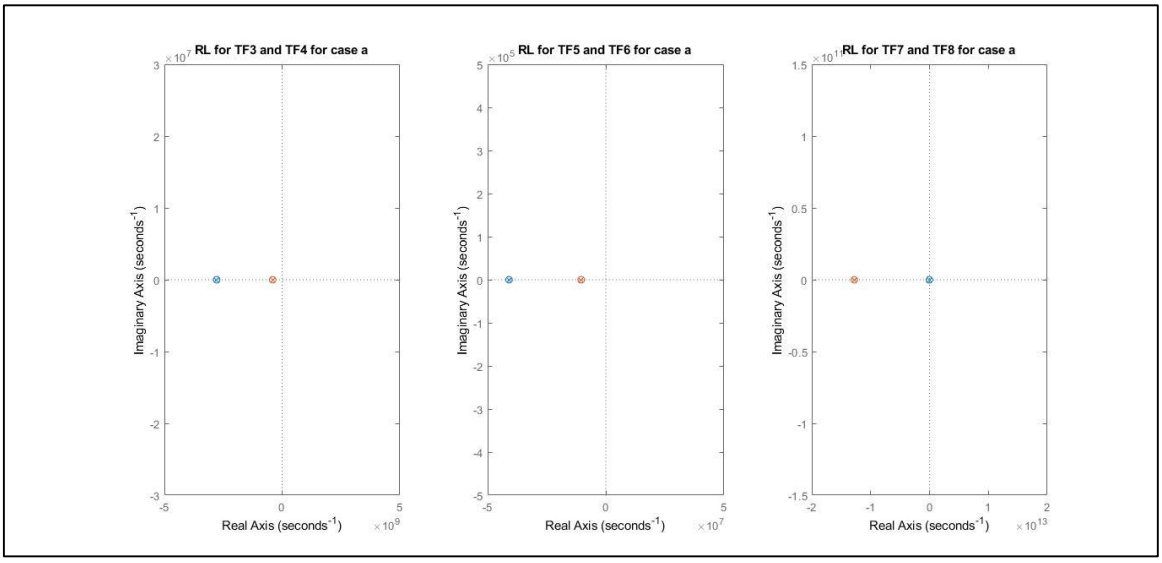

Figure 2. 7: Root locus from TF3 to TF8 for case ‘a’.

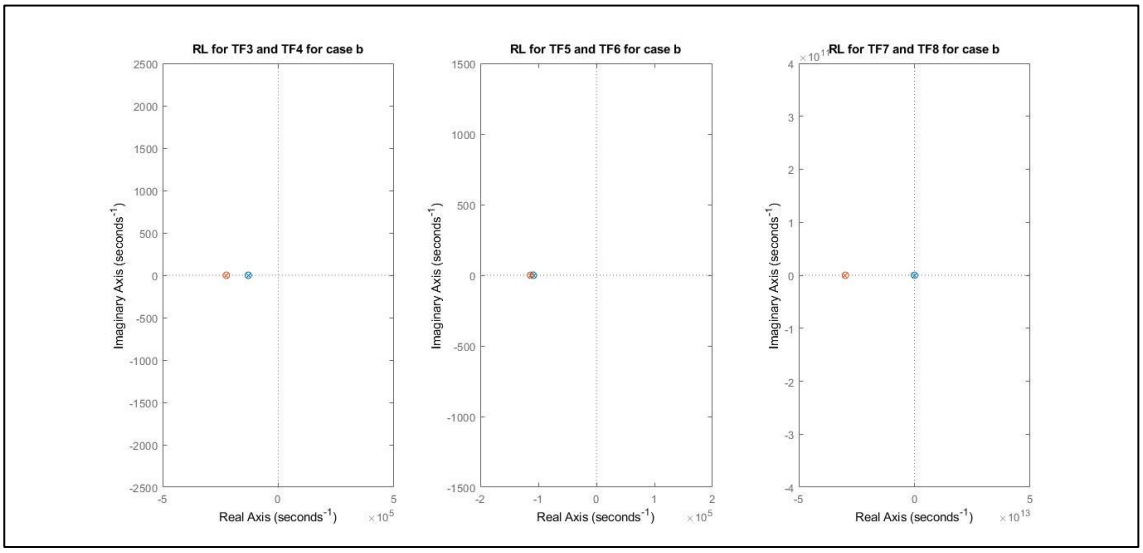

Figure 2. 8: Root locus from TF3 to TF8 for case ‘b’.

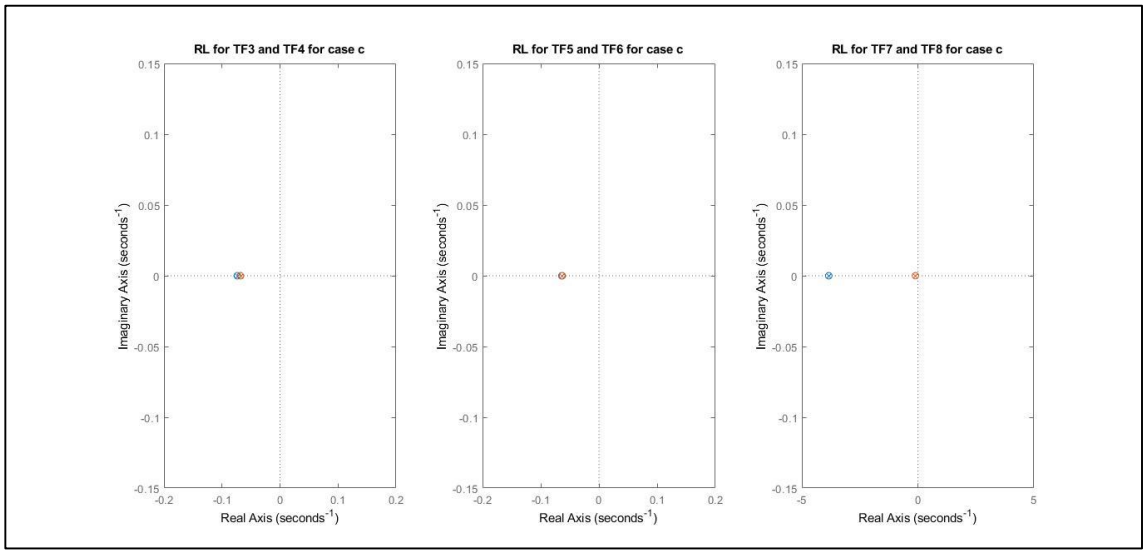

Figure 2. 9: Root locus from TF3 to TF8 for case 'c'.

The heater block is stable for all ranges of gain. It is noticeable that the root locus of TF_1 for all fan speeds have two asymptotes at a phase angle of 180º. Also the root locus suggests that the effect of chain in gain values will be negligible for the heat sink block. The TF_2 for all the three cases have the pole very near to the imaginary axis. For case 'c' as seen in Fig. 2.6 the complex pole pair makes the system unstable as damping ratio is $\xi < 0$ in the right halfplane.

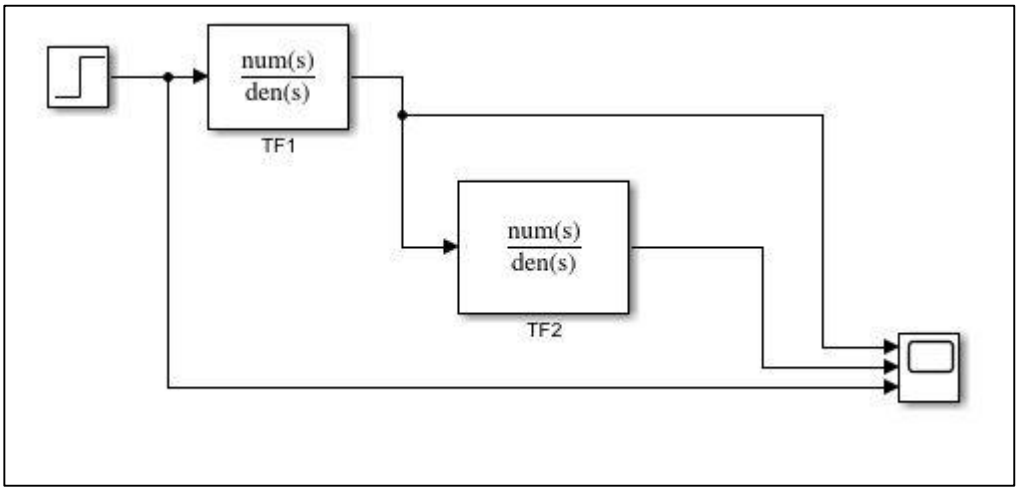

Figure 2. 10: MATLAB Simulink model to observe system response**.**

To observe the system response to a step input MATLAB Simulink was used for the TF_1 and TF_2 for different fan speeds. Under normal operating condition the load to the liquefier is going to be constant, so a step input will give a good representation of the system behavior. The MATLAB Simulink model in Fig. 2.10 is used to obtain the response, with a step height of 200 and step time at 1 sec. The response for TF_1 is shown in Fig. 2.11 and responses for TF_2 is shown in Fig. 2.12.

Table 2.4: Steady state error for a step input with set point 200.

	Case 'a'	**Case 'b'**	**Case 'c'**
TF_1	5.9312	5.7208	6.1104
TF_2	155.1	161.62	165.16

For a step input with step height of 200 to a system in Fig. 2.6, we obtain the steady state error as shown in Table 2.4. It is clear that the temperature of the heat sink will be always within 25% of the temperature of heat block.

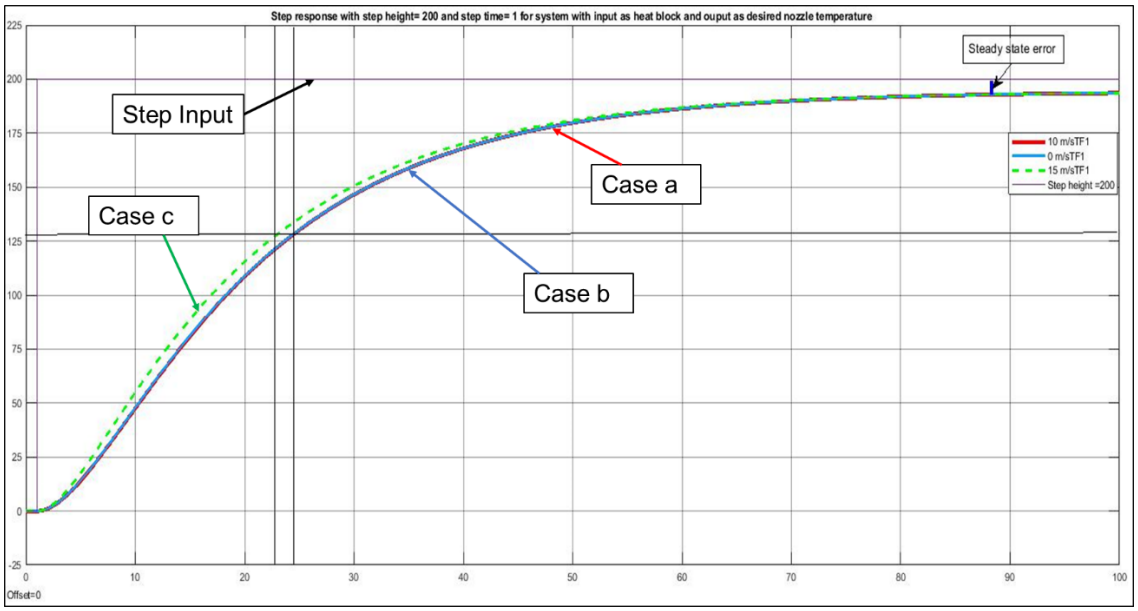

Figure 2. 11: System behavior as step response for TF1.

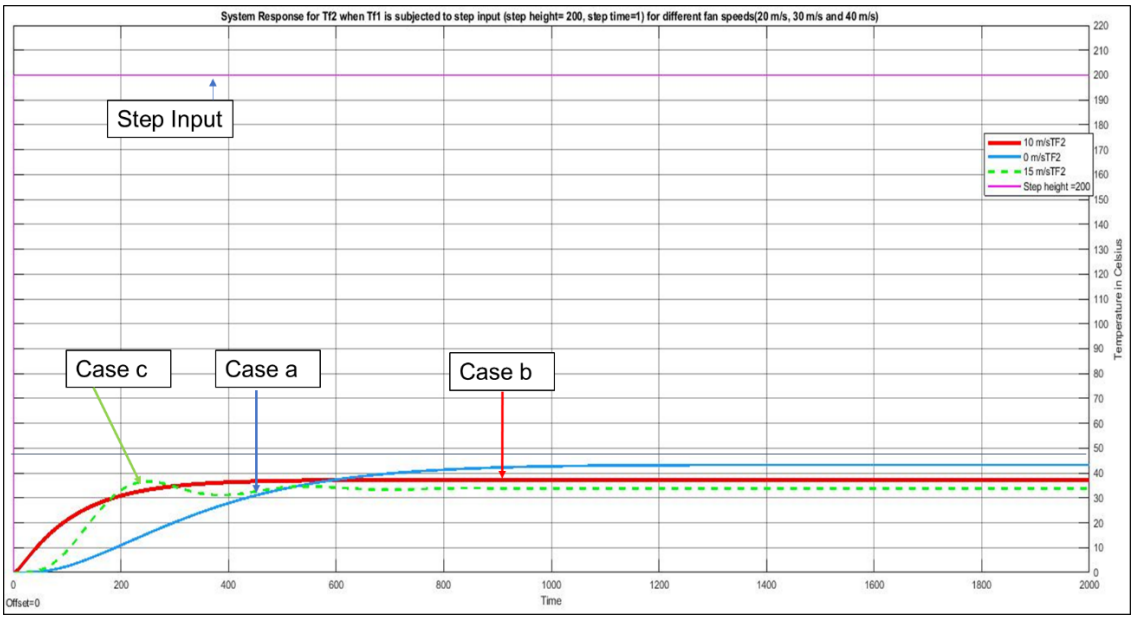

Figure 2. 12: System behavior as step response for TF2.

The system response in Figure 2.11 suggests a compensation is required to reduce steady state error and response time. A closed loop system is modelled to simulate a feedback

control strategy to achieve a better response. The filament drive system as discussed earlier acts a load to the liquifier system. To account for this load, a constant load signal will be applied to the system. The system modelled in MATLAB Simulink is shown in Fig. 2.13. The compensator is tuned in Control System Designer app available in MATLAB. Two compensators are simulated,

1) Lead Compensator: $$C_l(s) = \frac{292.4(s+0.3726)}{(s+3.458)} \quad (2.9)$$

2) Lead-Lead Compensator: $$C_{ll}(s) = \frac{39300(s+0.3726)(s+1.058)}{(s+1.356)(s+39.08)} \quad (2.10)$$

The system stability after addition of compensation remains stable as seen in Fig. 2.14 and Fig. 2.15. The system response of the system modelled in Fig. 2.13 with plant transfer function as TF_1 from Table 2.1 are shown in Fig. 2.16.

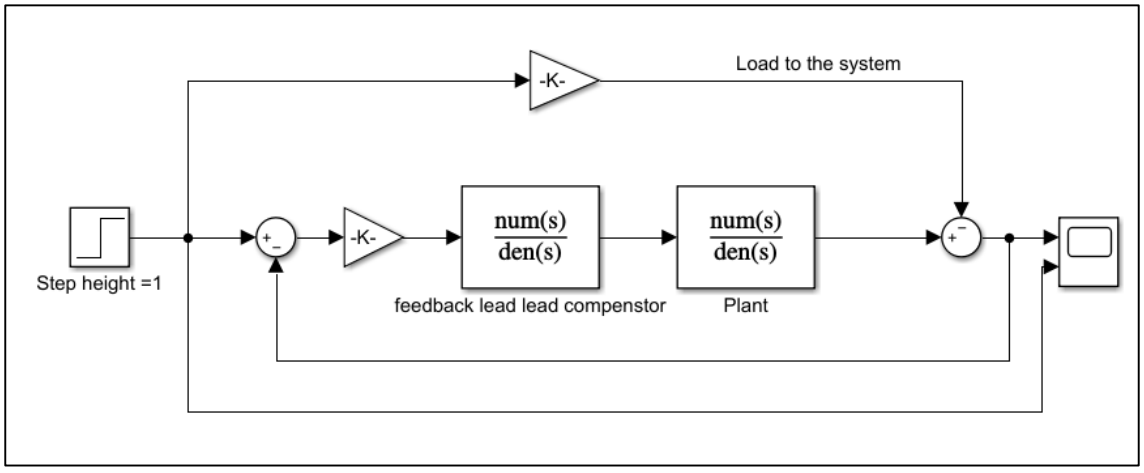

Figure 2. 13: MATLAB Simulink model for temperature control of liquifier block.

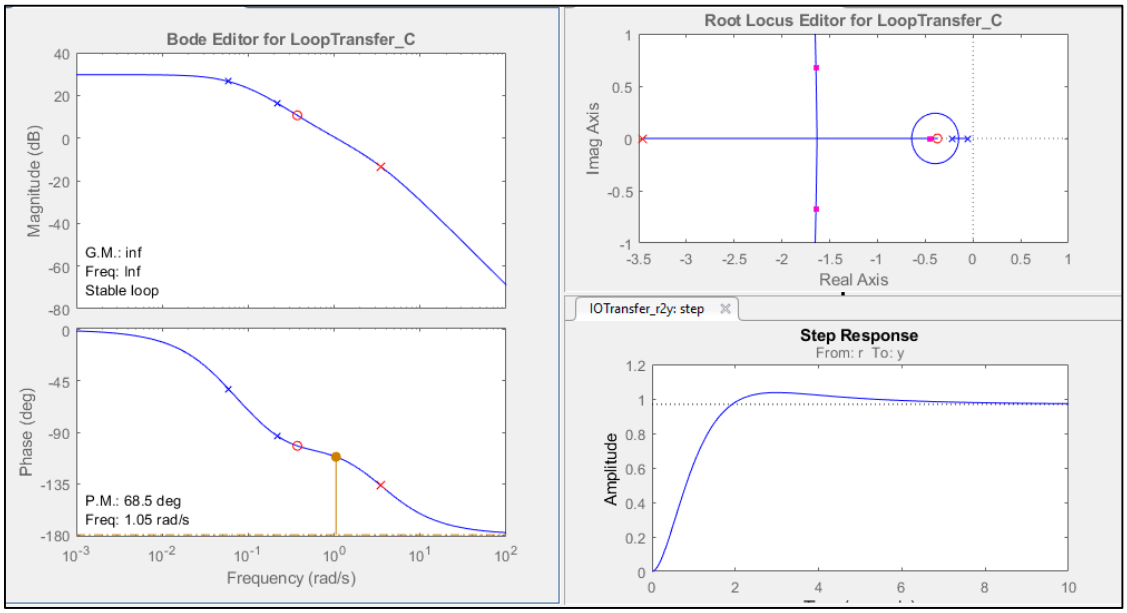

Figure 2. 14: System response, Bode plot, and Root locus plot after addition of a Lead compensator.

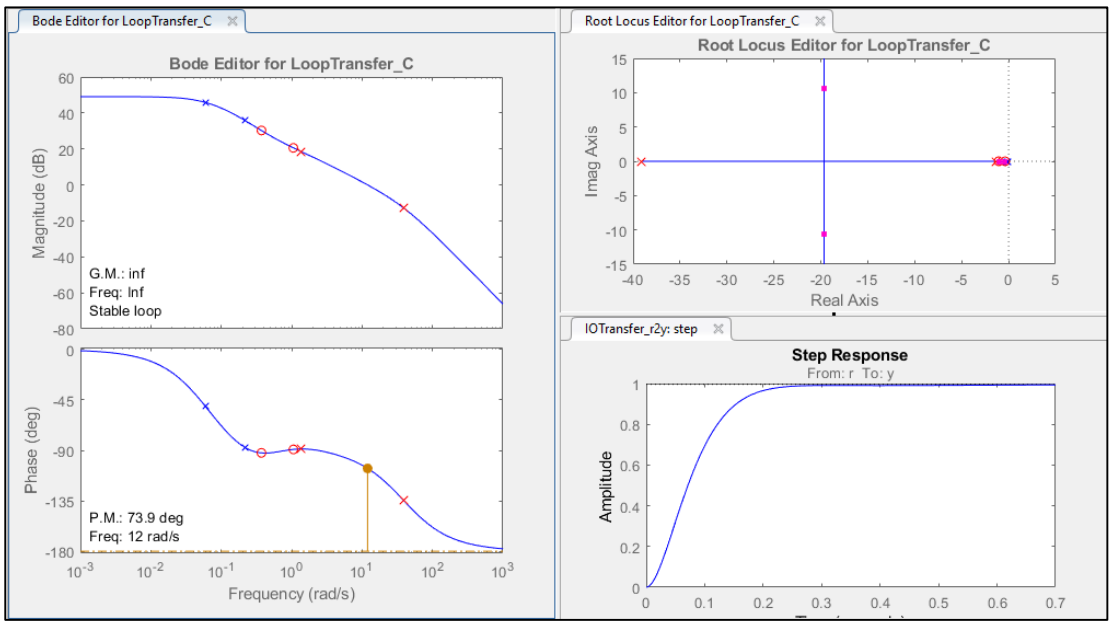

Figure 2. 15: System response, Bode plot, and Root locus plot after addition of a Lead-Lead compensator.

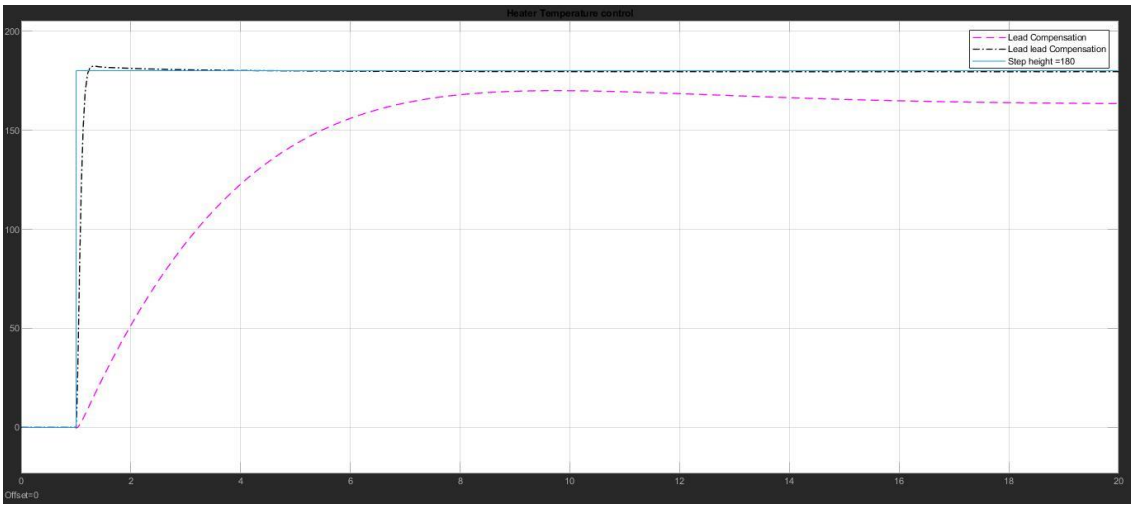

Figure 2. 16: System response comparison for both Lead and Lead-Lead compensators.

The system response shows that the lead-lag compensator has negligible steady state error and very low settling time. It does show an initial spike, but it is controlled within one-time unit. The lead compensator does not show an initial spike but has higher settling time and larger steady state error.

Chapter 3

PROCESS CONTROL IN LASER BASED METAL ADDITIVE MANUFACTURING

Metal additive manufacturing (AM) covers a wide range of methods that are typically performed in layer-by-layer building format. Metal AM technologies such as Laser Metal Deposition (LMD), Laser Powder Bed Fusion (L-PBF) are suitable for customization of medical products, repairing/ replacing aging parts or direct part fabrication for aerospace, marine, and energy applications. The quality of the process and/or the product involves criteria that are related to reliability, durability, serviceability, aesthetics, and compliance to certain standards (O'Regan et al. 2016). In many industries such as aerospace applications where retaining mechanical properties is also a must as part of design requirements, large variations in fabricated part properties, and structural integrity prevent metal AM technologies from replacing most traditional manufacturing technologies.

In a Laser Metal Deposition (LMD) system, several important steps occur that affect the way the part is manufactured:

i) the part computer-aided design (CAD) geometry is oriented in the build volume and sliced into layers with certain layer thickness, ii) the slices are then imported into a build preparation software that allows the user to specify the exact location of these slices on the substrate, iii) a set of processing parameters (laser scan velocity, laser power, hatch spacing, etc.) are specified in the software, and iv) laser beam path corresponding to the

selected hatch pattern is generated for every layer based on the part location on the build area, and the specified processing parameters.

3.1 Process Parameters and Variables

In the literature of laser-based AM processes, one of the highly exploited quality measures is the density of the final product (Kempen et al. 2011; Kamath et al. 2014; Mertens et al. 2014; Kamath 2016). Surface roughness and dimensional tolerances are other common quality measures (Kempen et al. 2011; Kamath 2016). Melt pool geometry is also widely studied due to being a determinant of density and surface roughness (Kempen et al. 2011; Lopez et al. 2016). Kamath (Kamath 2016) claims that small melt pool depths make the system inefficient by increasing the processing time. On the other hand, large melt pools may yield vaporization of the substrate and causes pores in the structure that increase porosity (Montgomery et al. 2015). To insure a stable melt pool, the melt pool dimensions are not allowed to be too small or too large in order to avoid irregularities or droplets (Mertens et al. 2014). O'Regan et al. (O'Regan et al. 2016) classifies these parameters under four groups: (i) feedstock related, (ii) build environment related, (iii) laser source related, and (iv) melt pool related. Most of these parameters are predefined, that is, their values have to be adjusted before processing and some are controllable, that is, their values can be changed during processing. Lastly, some criteria are classified as undefined, that is, their values depend on other parameter adjustments. Control and optimization over LMD systems are achieved by changing predefined and controllable parameters. Even though laser power P, scan velocity v_s , hatch distance h and layer thickness t_{layer} have been known to be most important parameters through experimentations, their relative importance are statistically analyzed in the recent study of Kamath (Kamath 2016). According to this

study, scan velocity is the most important parameter. High scan velocity causes the interaction between materials and the laser to be short, which results in a narrow melt pool which also leads to rough surfaces, whereas decreasing the scan velocity causes vaporization. Very high scan velocity causes instability and droplet formation due to free cylindrical melt pool geometry. Very low scan velocity yields distortion and irregularities due to balling effect and it is advised that 600-700 mm/s (Kempen et al. 2011). Low scan velocity is known to ensure a dense structure with the cost of rough surface. Hence, the optimal scan velocity is a trade-off between density and surface quality (Mertens et al. 2014).

A fuller understanding of the LMD and L-PBF processes is highly crucial to develop process control for rapidly qualifying and certifying the quality of the additively fabricated parts. In that regard measurements at pre-process, in-process, and post-process stages are required. Basically, pre-process measurements are vital in establishing relationships between input process parameters and part characteristics. These measurements often relate to material properties (density, thermal conductivity, etc.) and intrinsic characteristics of the system (laser power, feedstock rate, powder absorptivity, etc.). In-process measurements are typically in-process monitoring tools such as measuring surface temperature, monitoring melt pool shape and size, and spatter of the molten powder material (Criales et al. 2017; Arisoy et al. 2019). There are certain difficulties to monitor the process in LMD including the emissivity of the imaged object with thermography and metallic debris or spatter from the heat-affected-zone that can cover the viewport of the thermal imaging system and disturb temperature measurements (Mani et al. 2015; Arisoy et al. 2017).

It is stated that being able to characterize the process signatures of LMD process is key to improving the product quality. The post-process measurements have in general focused on the part quality and are based on the following categories: dimensional accuracy, surface topography, surface roughness, porosity, mechanical properties, residual stress, and fatigue (Özel et al. 2018b).

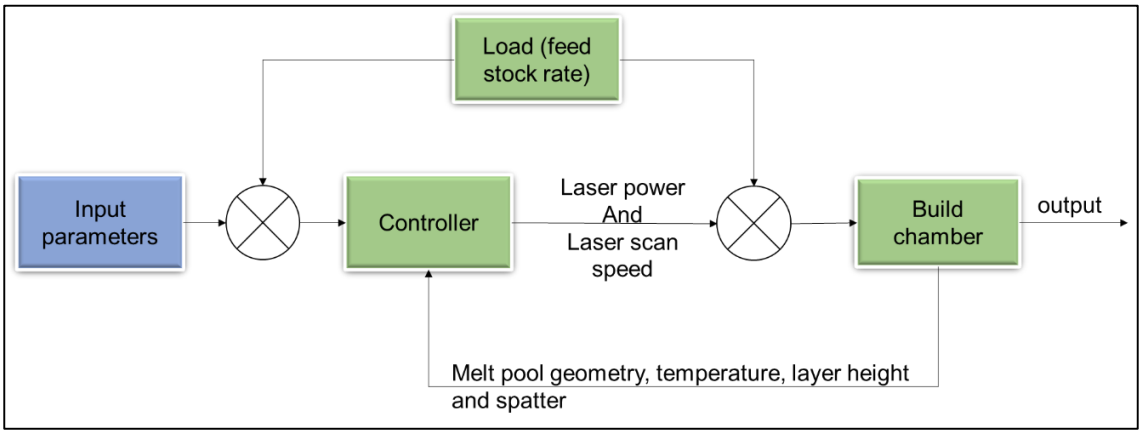

Figure 3. 1: Overall control scheme.

To establish foundations for process control, process parameters are sub-categorized as process signatures and product quality according to the abilities to be measured and/or controlled. Process parameters are input to the LMD process and they are either potentially controllable or predefined. This overall approach is summarized in Figure 3.1.

In this control scheme, predefined input parameters are given as set parameters and they will include factory specified feedstock related parameters such as powder material particle size or wire , and LMD equipment specific parameters such as layer thickness, shielding gas flow rate, and ambient gas environment etc. e.g. $\underline{r} = [r_1, r_2, \dots, r_n]^T$. We will consider them as uncontrollable inputs and thus parts of the parameters of uncertainty. Controllable parameters including laser power and scanning parameters e.g. $\underline{u} = [u_1, u_2, \dots, u_m]^T$are

often used to control the heating, melting, and solidification process and thus control the part quality. Controllable process parameters generally correlate to the observable and derived process signatures such as melt pool size, temperature, layer height, porosity, distortion or residual stress. Derivable parameters cannot be directly measured but can be calculated using numerical models (Criales et al. 2017). For purposes of correlations we further subdivide the process signatures into three categories namely: melt pool, re-solidified melt track, and fused layer (Arisoy et al. 2019). Process signatures determine the final product qualities (geometric, mechanical, and physical). Developing correlations between the controllable process parameters and process signatures should support process control, with the goal of embedding process knowledge into future control schemes.

The quality of build components in LMD are influenced by a large number of process parameters that need to be well-identified to optimize build quality. It is widely accepted that the build quality can be improved by minimizing the formation of material discontinuities. A wide range of material discontinuities can occur such as void and/or pore formation where shielding gas pores are entrapped within the bulk metal during solidification and these pores are affected by the degree of melting and boiling the molten material. Gas bubbles can be trapped in the powder layer when laser power is low while high power causes excessive evaporation and turbulence that generates gasification. The solidified grains tend to be equiaxed in shape while those that form from the incomplete consolidation between layers are elongated (Arisoy et al. 2016). Balling is another discontinuity caused by high laser power that causes oxidation and sphere formation larger than the layer thickness during solidification.

Some of the methods used in collecting measurement data are summarized below:

In-Line Cameras are used to measure the dimensions of the melt pool, movement of dynamic melt pool, movement of the dynamic melt pool, and the mean radiation emitted in the area with a goal to reduce the occurrence of over-melted zones and resulting spherical pores. A typical resolution is in the range of 10 microns to 20 microns per pixel (Özel et al. 2018a).

Li et al. (2018) proposed an enhanced phase measuring profilometry (EPMP) to measure the 3D surface topography of the melt-pool. With his 3D contour monitoring of the fusion area he concluded that manufacturing accuracy of the workpiece at the center is higher than that of the edges. The standard deviation of layer height increases with increase in laser power. Hoffman et al. (2012) measured the meltpool dimensions and established a feedback control system.

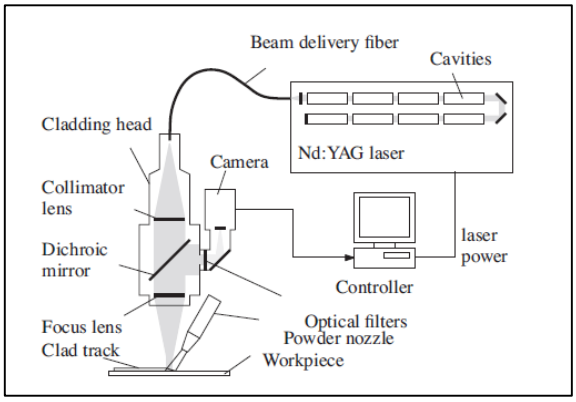

Figure 3. 2: In-line camera process monitoring system (Hoffman et al. 2012)

Pyrometry is employed for in-process measurement of process temperature and melt pool characteristics with a goal to monitor and control melt pool geometry by correlating melt pool size with layer thickness. Typically, the field of view is limited, and slow data

acquisition rates and laser radiation distort images and material vaporization and laser spatter create high level of noise in the imaging zone.

Infra-red (IR) Imaging is another in-process measurement technique that has reasonably good accuracy and offers higher capture rates. IR is capable of measuring thermal gradients during heating and cooling to evaluate heat dissipation irregularities or other discontinuities. A major issue with IR camera imaging is accumulation of vapor and debris on the optical lens' surface if the system is employed in a chamber. Then, there is a trade-off between field-of-view (FoV) versus resolution that can be avoided by external mounting of the IR camera and employing long range optics.

Optical Scanning

In the LMD process the laser deposition head move along the product design path. This makes optical scanning a better choice as an inline sensor. Using optical triangulation method Donadella et al. (2018) and Heralic et al. (2012) measured the continuous layer height. The optical triangulation method uses the light reflected by the build surface and uses them to detect the height variation and creating a spatial height map.

3.2 Process Control Strategies

The closed loop control for the process requires the system characteristics equation. To directly obtain mathematical relation between process parameters such as laser power, laser scan speed, melt pool dimensions and layer height involves complex equations. Hoffman et al. (2012) used experiments, identification and control methods to implement feedback control. In that research the melt pool images were smoothen, thresholded and estimated as an ellipse to obtain the melt pool width. As the dynamic relation between the laser power

and the width of the melt pool is non-linear, to linearize them only the low frequency dynamics and generated plant function using Autoregressive exogenous model as follows, where, $y(t)$ is the melt pool width, $u(t)$ is the laser power and $e(t)$ is process noise. The quantity (t) means the signal $y(t)$ is evaluated at its previous sample number, i.e.$y(t - t_s)$, with $\mathrm{t_s}$ the sample time. The ARX model is expressed in the frequency domain for the plant transfer function as:

$$G(s) = \frac{Y(s)}{U(s)} = K\frac{1}{\tau s+1} \tag{3.1}$$

They used A Proportional integral controller with a Low Pass Filter (LPF) to achieve zero steady state error. And the closed loop transfer function $C_{cl}(s)$ was given as follows

$$C_{cl}(s) = \frac{C(s)\,G(s)}{1+C(s)\,G(s)\,LPF(s)} \tag{3.2}$$

Where $C(s)$ is the controller function, $LPF(s)$ is the Low pass filter and $G\,(s)$ is from Equation 3.2. This developed camera-based feedback control system adjusted the laser power in real time to manipulate width of the melt pool at a user define reference value.

Heralic et al. (2012) and Hagquist et al. (2014) emphasized their research on Wired Laser Metal Deposition (LMD-w) to control the layer height and obtain a flat surface in each layer. In the open-loop case, for each new layer, the robot's tool center point (TCP) is offset by an estimated layer height in the z-direction. They used feedforward control strategy using iterative learning control (ILC) algorithm to control the layer height and reduce excessive deposition during sharp corners. Heralic et al. (2012) used optical triangulation principle to obtain real time layer height for monitoring and control. Hagquist et al. (2014) used a resistance-based system instead of optical scanning to achieve the same objective

but reducing the equipment cost, but can only be used for a metal wire (good conductor of electricity) based LMD.Their plant dynamics model used height change as a function of Δv_w(deviation around the nominal wire feed rate v_w) and time. They used the data of the last two iterations to estimate the input variables for the next layer. The iterative learning control schematic developed by Heralic et al. (2012) can be seen in Fig. 4.4. The plant transfer function used is similar to Eq. 3.1 with only difference in gain value (K) and time constant (τ) as the plant function is the first order approximation from the wire feed rate to the bead height. The controlled input using ILC controller given by Heralic et al. (2012) is as follows,

$$u_{j+1}(k) = Q(q_k)[u_j(k) + q_k^d(\gamma_1 e_j(k) + \gamma_2 e_{j-1}(k))] \quad (3.3)$$

And $e_j(k) = \bar{h}_j + T_j^z - H_j(k)$ (3.4)

Where, $\bar{h}_j$ is the mean layer height , $H_j(k)$ is the total height of the deposited part in a single point, i.e. at time index k , after layer j has been deposited, and T_j^z as the robot's height at layer j. u_j is the control input that controls the wire feed rate on layer j, γ_i are the so called learning gains, and $Q(q_k)$, defined as the Q-filter, is a zero phase low pass filter based on a 2nd order Butterworth filter, in the time shift operator .Furthermore, a time shift operator, q_k^d, acts on the two error signals, $e_j(k)$and $e_{j-1}(k)$, where d denotes the number of samples the corresponding signal is shifted in time.

The previous studies have either focused on the layer height or the feedstock control. This system still needs research to improve the process control for a quality product.

Chapter 4

CONTROL STRATEGIES

We investigated several control strategies that are used in additive manufacturing processes. These strategies include process monitoring and control that is related to temperature monitoring of the process, feedback control of measured variables, feedforward control of motion trajectory, and learning control and repetitive control strategies. A general framework of a control system is shown in Fig. 4.1 where process, controller with feedforward compensator and feedback controller are shown. The process is also considered as affected by disturbances. A summary of control strategies is listed in Table 4.1.

Table 4. 1 A summary of control strategies used in AM.

Process	Control Strategy
Fused Filament Fabrication	Process Monitoring and Control, Feedback Control
Directed Energy Deposition	Process Monitoring and Control, Feedback and Feedforward
Laser Metal Deposition	Process Monitoring and Control, Feedback and Feedforward
Laser Powder Bed Fusion (L-	Process Monitoring and Control, Feedback and Feedforward

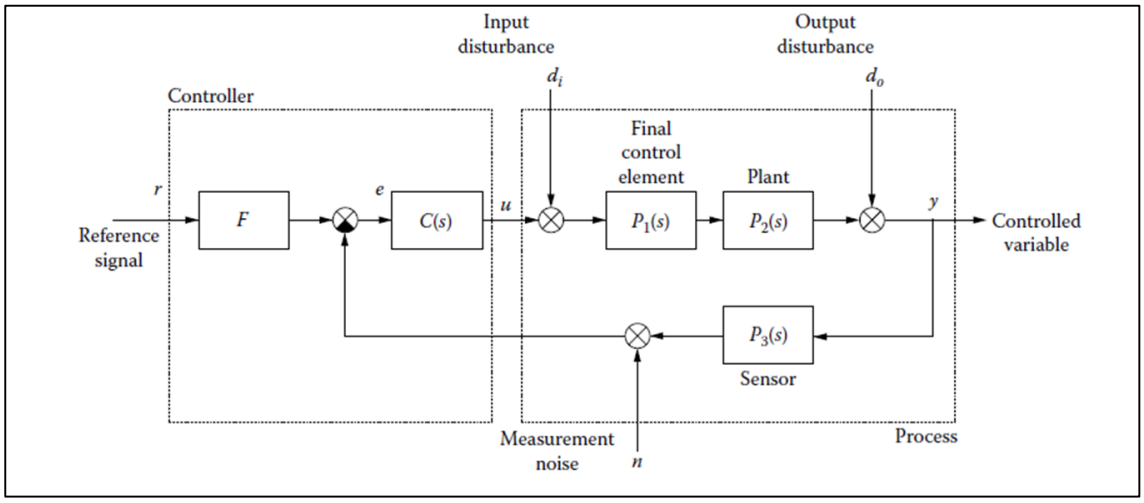

Figure 4. 1: A general framework for control strategies.

4.1 Feedback Control Strategies

The feedback strategy is very similar to the actions of a human operator attempting to control a process manually. Consider the control of the heat block in the FFF process. The operator would read the temperature sensor reading of the heat block and compare its value with the temperature desired. If the temperature was too high, the operator would reduce the value of input temperature of the heat block, and if the temperature was too low, the operator would increase it. Using this strategy, the operator would manipulate the input temperature valve until the error is eliminated.

A feedback control strategy as seen in Fig. 4.2 was used by Jason et al. (2016) for a L-PBF process. As shown Fig. 4.2, a single input parameter is the laser scanning trajectory which is neither manipulated nor controlled while the system is in operating mode. The input variables or the controlled variables are laser power and laser scan speed. The scanning trajectory is a predefined input but allowing the laser scan speed to be manipulated gives

us a better control during sharp corner turns in the layer geometry to achieve the desired shape with high precision.

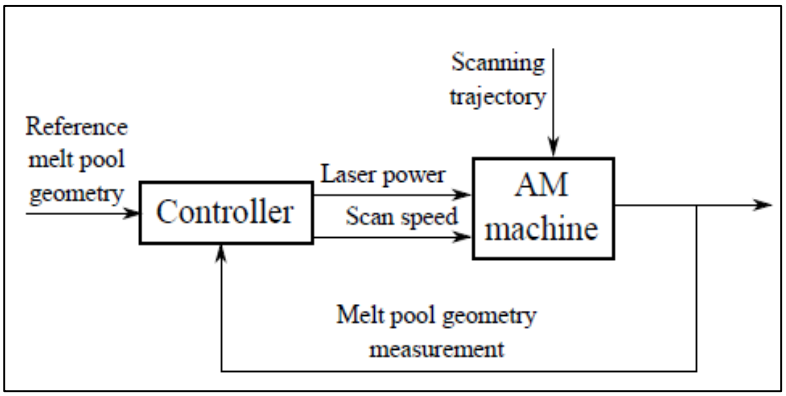

Figure 4. 2: Feedback control used for laser-based AM

by Jason et al. (2016).

Most authors focused on laser power and melt pool temperature and intensity for controlling the L-PBF or LMD. For example, a feedback control strategy has been introduced to LMD by Hassler et. al (2016).

4.2 Feedforward Control Strategies

The feedforward strategy provides a more direct solution as it does not rely on the error signal of the manipulated variable (as in feedback control). The feedforward system focuses on balancing the manipulated variable against the load, providing the forward loop with compensating dynamic elements. Considering the processes discussed in the earlier chapters a generalized framework can be seen in Fig. 4.3. The manipulated variable in laser-based AM processes is usually laser power (Jason et al. (2016), Hassler et al.(2016), Hoffman et al. (2012)) and/or laser scanning speed (Jason et al. (2016)). The feedstock rate

is kept constant in FFF and LMD but it can certainly induce disturbances. In Laser Metal Fusion (LMF) the re-coater is responsible for transporting the feedstock from storage cylinder to the build cylinder. When the base of storage cylinder fails to elevate as desired it is a case of undesired load change (more feedstock or no feed stock). Similarly, in the filament drive block of FFF process if the filament breaks or get stuck in the pinch rollers for even a few seconds there will be deformities or gaps in the final object.

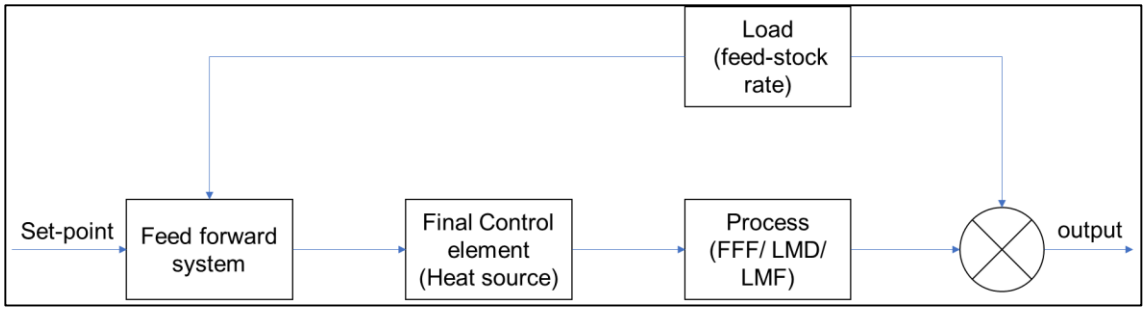

Figure 4. 3: A sample feedforward strategy

This strategy employs a system instead of a single control device. The feedforward system consists of several devices if implemented in hardware or several blocks of software if implemented digitally. The function of these blocks is to implement a mathematical model of the process. This strategy considers the instantaneous load (feedstock) on the system to manipulate heat source (heater (FFF), laser power (LMD, LMF, L-PBF) to control the melt pool signature.

4.3 Learning Control Strategies

This process control strategy includes learning algorithms which takes control action based on the analysis of past data. This control strategy can be employed only for offline mode, which means it is not quite useful for controlling parameters which are to be controlled

while the process is ongoing. Heralic et al. (2012) controlled the layer height by manipulating the feedstock rate using Iterative learning controller (ILC). Laser scanning using the principle of optical triangulation was utilized to obtain the height profile of each layer. The iterative learning control attenuated the height deviations by controlling the wire feed rate and a step height compensator adjusted the robot position to compensate the wrongly estimated layer height. Hagquist et al. (2015) also used iterative learning approach using a resistance-based system to determine the height profile.

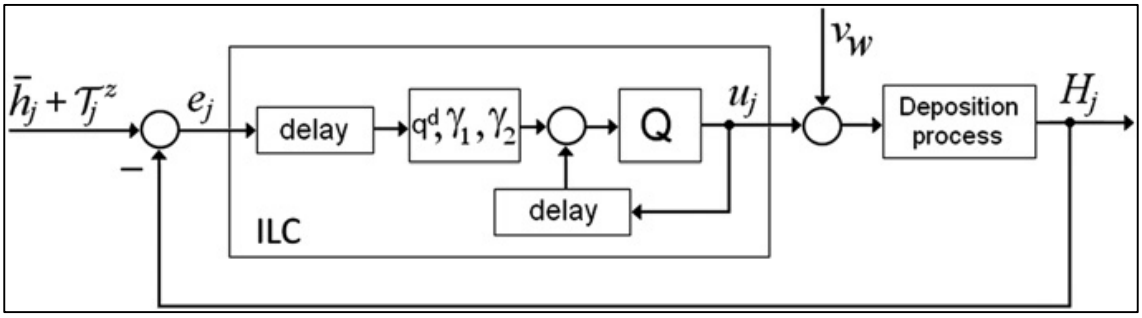

Figure 4. 4: A sample learning control strategy [Heralic et al (2012)].

Both publications have used ILC for attaining required layer height. This strategy can be used for controlling the XY positioning table for an Additive Manufacturing machine. This strategy for trajectory tracking will be discussed more in the next chapter. The ILC algorithm has proven to be useful when we experience constant disturbance.

Conditions for using ILC: The below listed conditions are crucial and only when they all apply, the ILC strategy can be used: (i) The system is asymptotically stable in closed loop, (ii) The trajectory is limited in time. (iii) The errors are reproducible, (iv) The initial conditions are same for every run. (v) The same trajectory is run repeatedly.

As described in the book by Chris et. al. ILC can be modelled with certain initial conditions and the terminology as discussed in this paragraph. When ILC is applied to discrete dynamics the notation used for a scalar or vector valued variable in this monograph is $y_k(p), p = 0, 1, \ldots, T$. Here the non-negative integer k is the trial number and $T \in$ N denotes the number of samples on each trial, with the assumption of a constant sampling period. Suppose also that the dynamics of the system or process considered can be adequately modelled as linear and time invariant. Then the state-space model of such a system in the ILC setting is; where on trial k, $x_k(p) \in$ R^n is the state vector, $y_k(p) \in$ R^m is the output vector and $u_k(p) \in$ R^l is the control input vector.

$$x_k\,(p+1) = A\,x_k(p) + Bu_k(p)$$

$$y_k\,(p) = C\,x_k(p), \qquad x_k(0) = x_0 \tag{4.1}$$

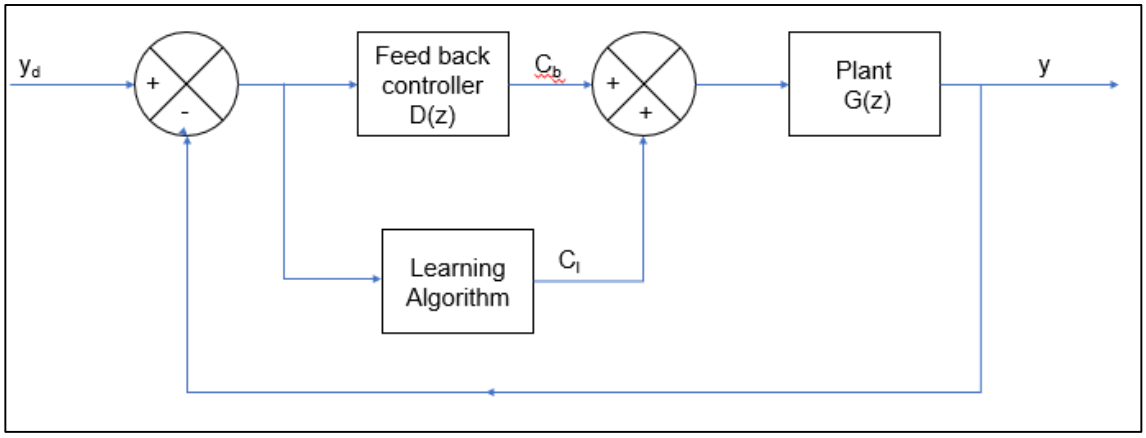

Figure 4. 5: A sample block diagram for iterative learning control strategy.

Consider the system in Fig. 4.5. The process input C consists of two components,

i) Feedback compensation: $C_b = D(z)E$ (4.2)

ii) Learning compensation: $C_{l,k+1} = C_{l,k} + R(z)E_k$ (4.3)

where $R(z) = D(z)$ is the learning filter.

Let $y_d(p) \in \mathrm{R}^m$ denote the supplied reference vector. Then the error on trial k is, $e_k(p) = y_d(p) - y_k(p)$ and construct a sequence of input signal $u_k + 1(p)$, $k \geq 0$, such that the performance is gradually improved with each successive iteration and after a 'considerable number of these iterations the current trial error is zero or within an acceptable tolerance. Mathematically this can be stated as a convergence condition on the input and error of the form,

$$\lim_{k\to\infty} e_k = 0, \qquad \lim_{k\to\infty} (u_k - u_\infty) = 0 \tag{4.4}$$

The ILC algorithm convergence helps us to determine when we can stop iterating and also to determine are the control performances demanded achievable without wasting time in iterating loops.

Chapter 5

PROCESS CONTROL OF POSITIONING SYSTEM

5.1 An XY Positioning System

An XY positioning system used in some AM machines and 3D printers that are similar to the CNC machines and other machine tools that use XY positioning systems. Most of the modern machines can achieve very high accuracy in point-to point machining with conventional controllers but they result in significant contouring error when machining contouring path or a motion trajectory. The contour error is defined as error component orthogonal to the desired trajectory. The contour error is a function of e_x (error in x axis), e_y (error in y axis) and q (inclination of contour with respect to x axis). It is given by:

$$e(t) = e_y(t)\cos q - e_x(t)\sin q \tag{5.1}$$

A trajectory is created using MATLAB as shown in Figure 5.1, the trajectory is shaped as a rhombus. The closed loop discrete time transfer function of an XY positioning system in a machine tool given by (Srinivasan and Kulkarni 1990) are as follows,

$$H_y(z) = \frac{0.0012\,z^3 + 0.0083\,z^2 + 0.0132\,z + 0.0062}{z^4 - 1.451\,z^3 - 0.121\,z^2 + 1.018\,z - 0.446} \tag{5.2}$$

$$H_x(z) = \frac{-0.0001z^3 + 0.0096\,z^2 + 0.0158\,z + 0.0061}{z^4 - 1.726\,z^3 + 0.449\,z^2 + 0.742\,z - 0.465} \tag{5.3}$$

Where $H_y(z)$ represents the closed loop transfer function of positioning system for y axis, similarly $H_x(z)$ represents the closed loop transfer function of positioning system for x axis.

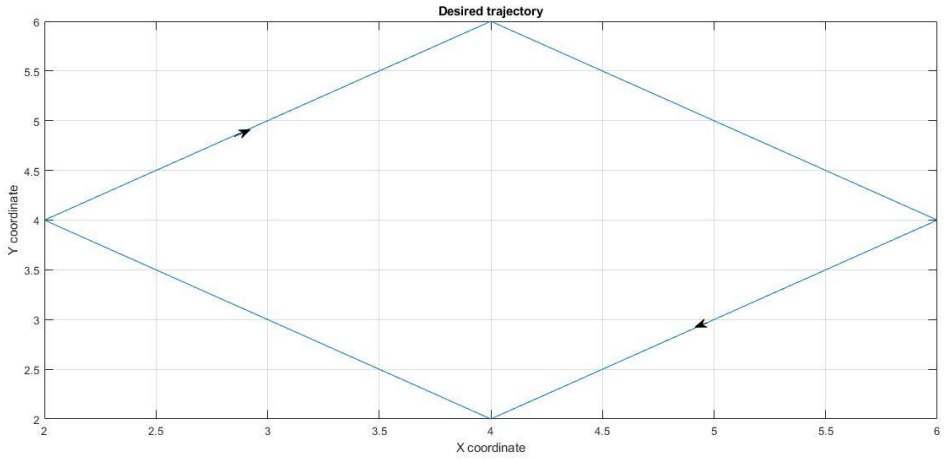

Figure 5. 1: Desired trajectory.

When the desired trajectory in Fig. 5.1 is given as an input to $H_x(z)$ and $H_y(z)$ the system response obtained is shown in Fig. 5.2. The sampling rate is kept T= 0.33 seconds and the simulation is done in MATLAB Simulink.

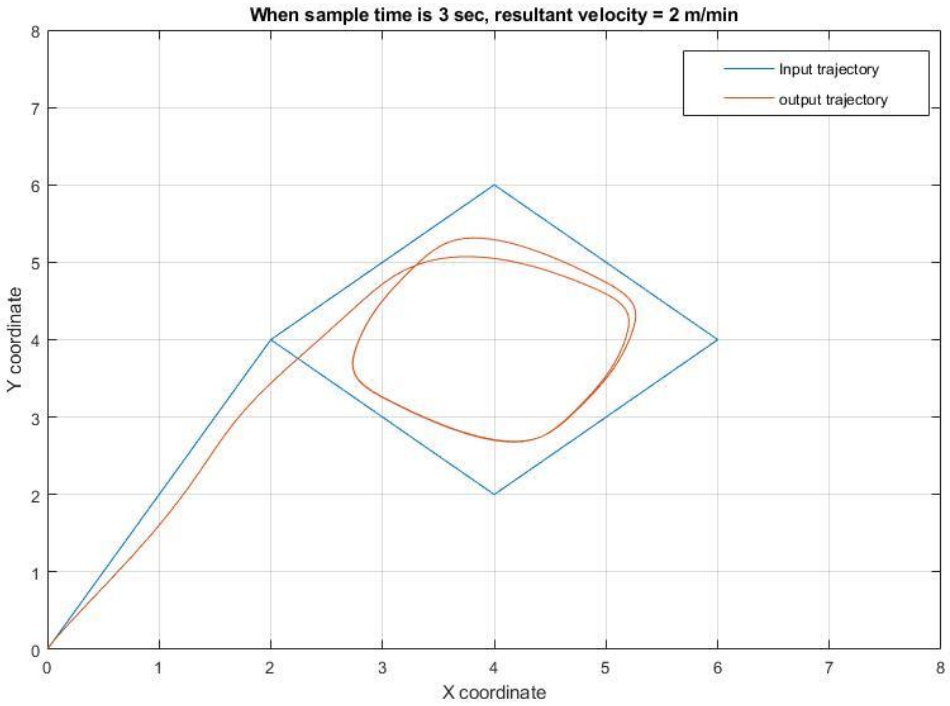

Figure 5. 2: Closed loop response of the XY positioning system.

The response in Fig. 5.2 shows a dire need of a controller. While this response was obtained, it was observed that the steady state response of the system has a huge steady state error. In order to investigate the stability of the closed loop transfer functions given in Eqs. 5.2 and 5.3, the root locus analysis was conducted and plotted as can be seen in Fig. 5.3. Both individual axis drive systems have either poles or zeros in the right half plane, implying that the system is unstable. But when the same trajectory is run periodically up to 4 or 5 periods it can be observed (Fig. 5.4) that the system is asymptotically stable at large.

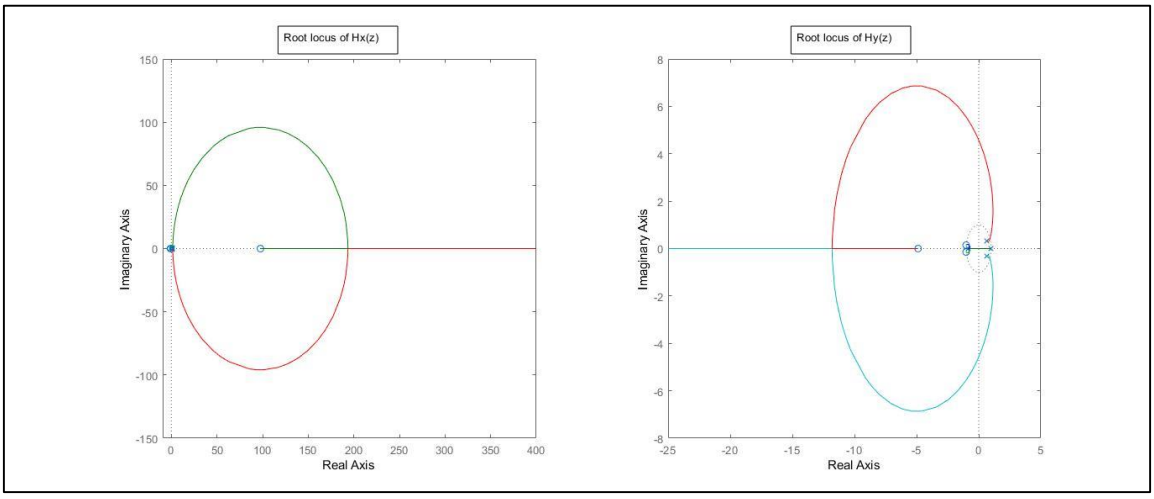

Figure 5. 3: Root locus analysis of the XY positioning system.

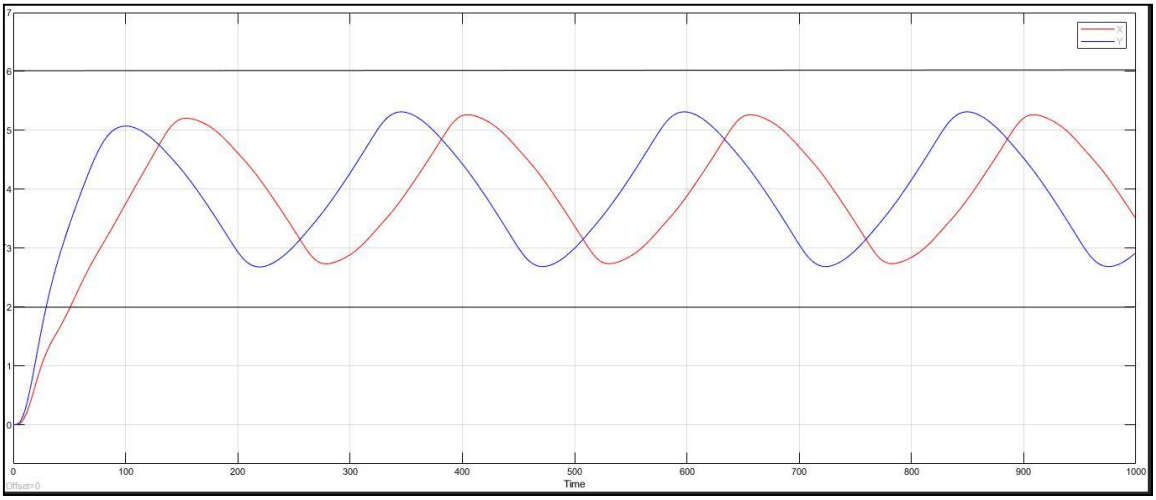

Figure 5. 4: System response over multiple periods.

5.2 Feedback Control

To stabilize the system initially a feedback compensator was designed using the Control System Designer App in MATLAB. A PID compensation tuning was used to improve the system response for a step input for both Equation 5.2 and Equation 5.3. The feedback compensator equations obtained are;

$$C_{fx}(z) = \frac{1.6331\ (\mathrm{z}-0.9684)}{(\mathrm{z}-1)} \tag{5.4}$$

$$C_{fy}(z) = \frac{1.2072\mathrm{z}-1.1791}{(\mathrm{z}-1)} \tag{5.5}$$

While this compensator reduced the error for a step response, for our required trajectory where not as expected. The Simulink model is shown in Fig. 5.5 and the system response is shown in Fig. 5.6.

The results are not satisfactory hence a more advanced controller is needed to remove the system errors. The closed loop response is asymptotically stable, the errors are reproducible (see Fig. 5.4) and trajectory is time bound (see Fig. 5.1). Therefore, an Iterative Learning Control scheme can be used to improve the system performance.

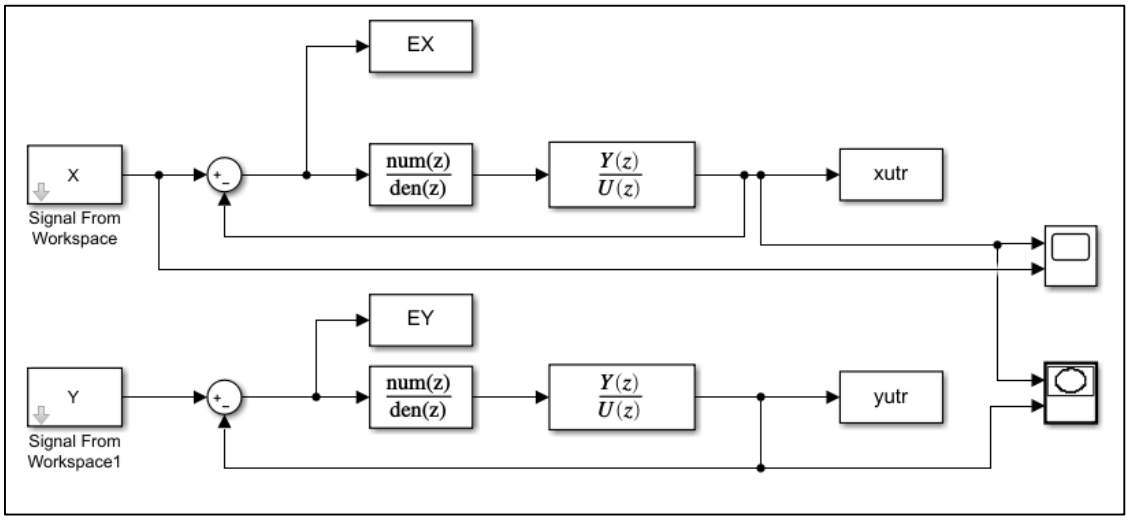

Figure 5. 5: MATLAB Simulink model for XY positioning system with Feedback control.

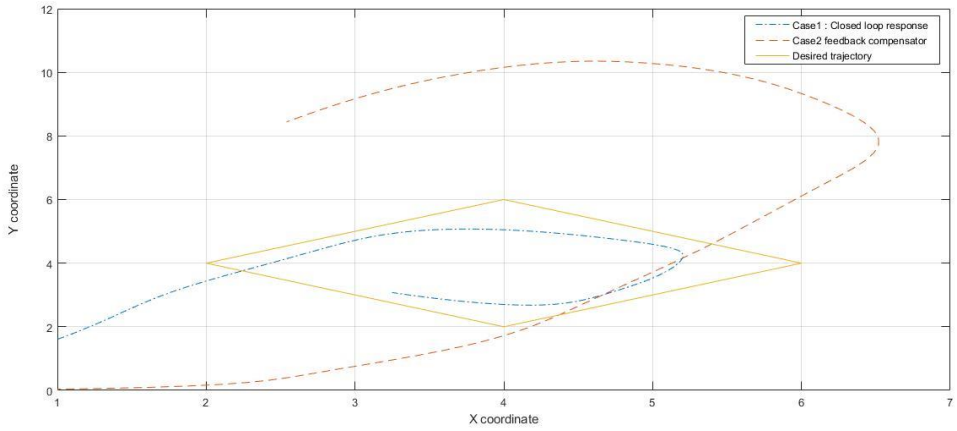

Figure 5. 6: Output trajectory obtained using feedback compensation.

5.3 Iterative Learning Control

As discussed earlier, the ILC conditions are satisfied by the system discussed in this section. Using the Eqs. 4.2, 4.3 and 4.4, a system was designed in MATLAB Simulink to obtain desired results. Also, in addition to the normal ILC algorithm the error $e_k(p-1)$ (where k is the iteration/trial number and p is the sample time) is also considered with a lower gain. The system model with ILC compensator is shown in Figure 5.7,5.8 and the system response is shown in Figure 5.8.

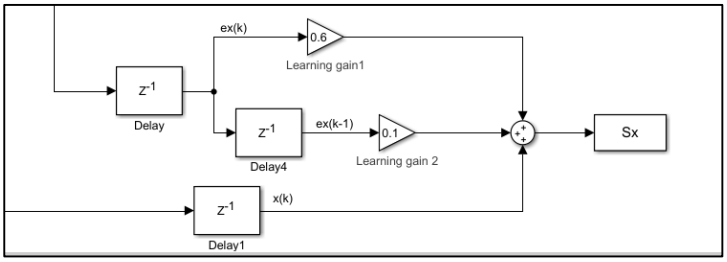

Figure 5. 7: The ILC compensator used for feed forward input.

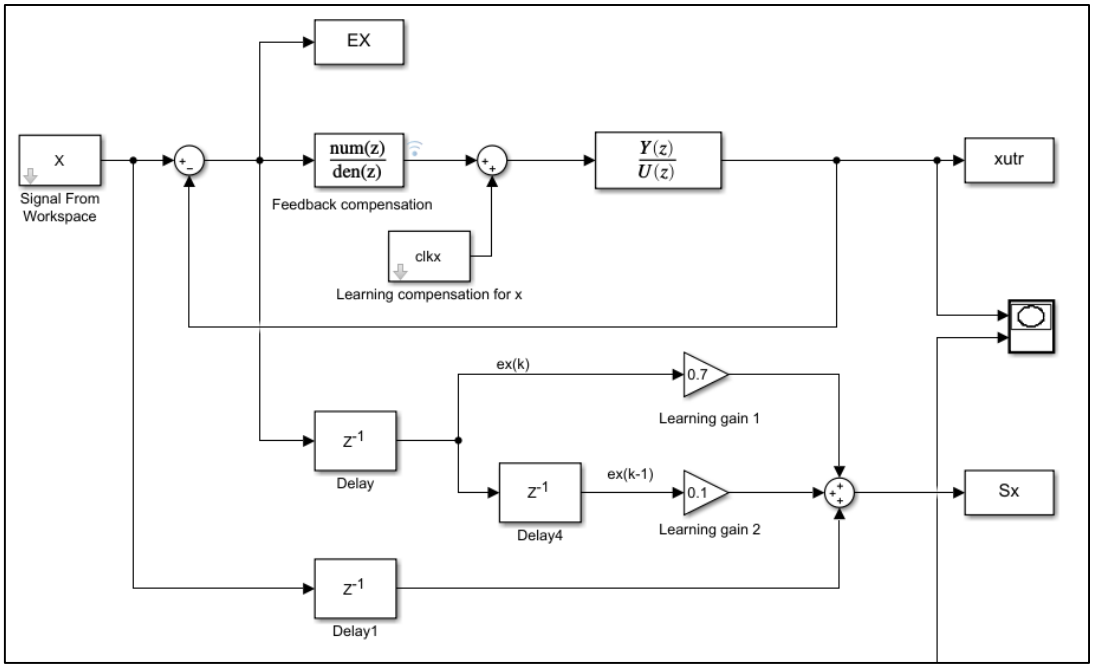

Figure 5. 8: MATLAB Simulink model with the ILC for x axis servo drive.

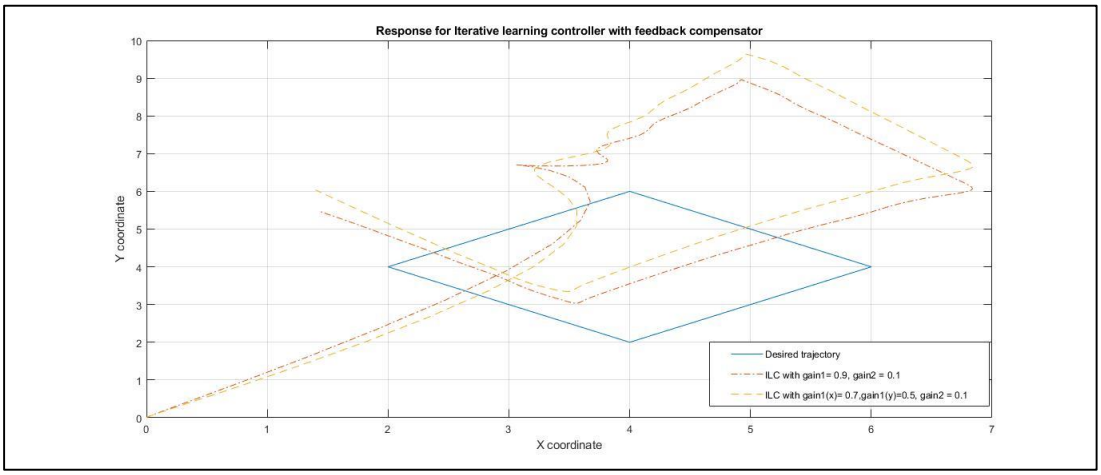

Figure 5. 9: System response of model for two different set of learning gain values.

Table 5. 1: Learning gain values used for the ILC model in Fig. 5.8.

		Gain1	Gain2
Case 1	x	0.9	0.1
	y	0.9	0.1
Case 2	x	0.7	0.1
	y	0.5	0.1

The ILC learning gain converged for both set of gains as shown in Table 5.1, but as we can see in Fig. 5.9 the response is still not as expected. To eliminate the system error more efficiently, the feedback compensator is removed and more values of gain where simulated. Also, there was an addition of two gains for each of the system just after the desired output and before the system output as shown in Fig. 5.10. These gains were added to such that they mathematically nullify each other's effect. If the initial gain is chosen as K = 400 than the final gain $K_2 = 1/K$ which is 0.0025 for this case. This is done so that we can achieve convergence faster and eliminate steady error quicker. As the

input is amplified to such a large magnitude, the error values become also large and provide a better system response. The system response can be observed in Fig. 5.11.

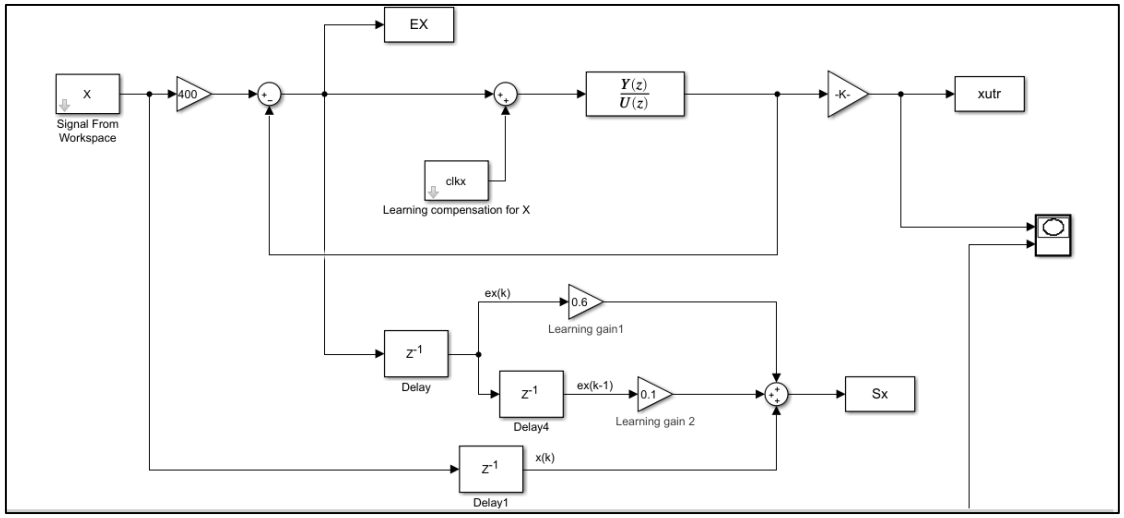

Figure 5. 10: Improved ILC model for the positioning system.

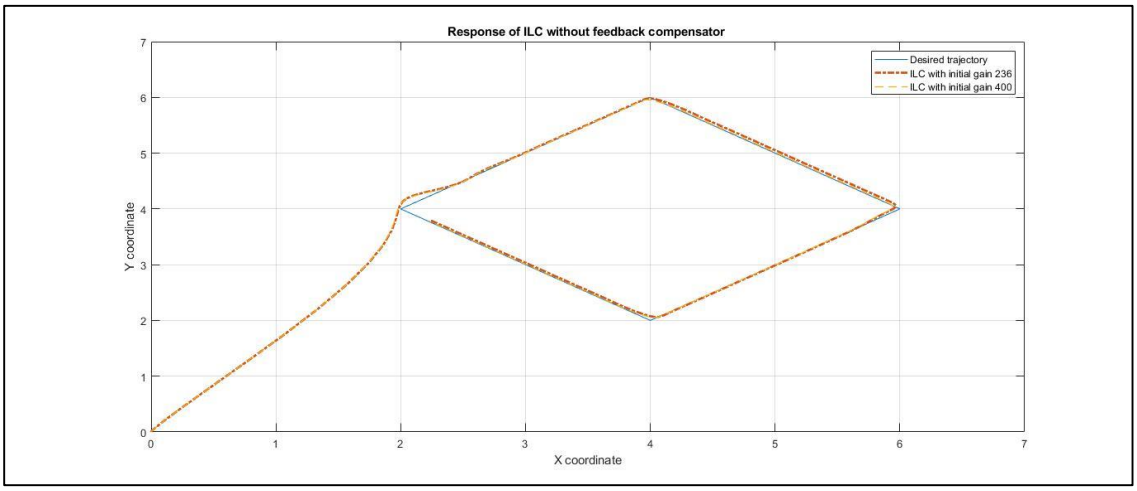

Figure 5. 11: System response for the ILC model in Figure 5.10.

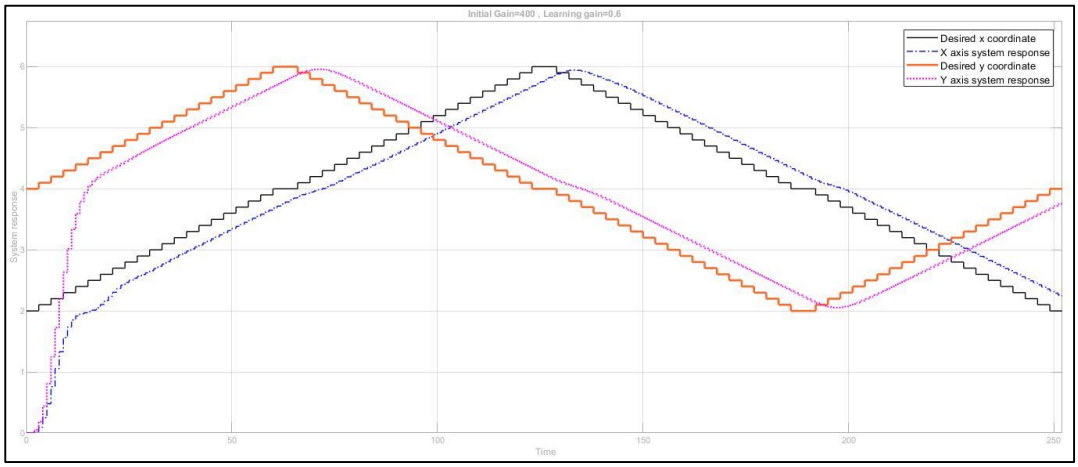

Figure 5. 12: System response for the ILC model in Fig. 5.10

(Case 1: Initial gain is 400).

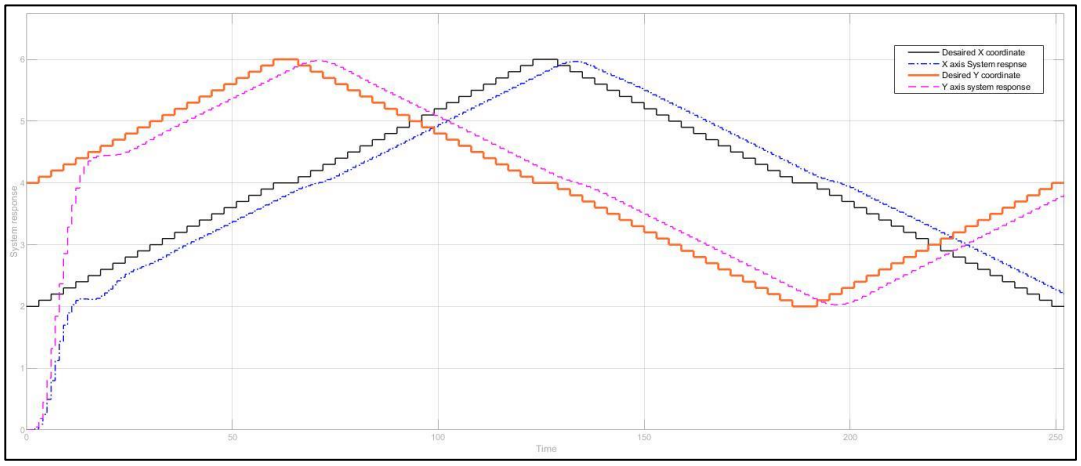

Figure 5. 13: System response for the ILC model in Fig. 5.10

(Case2: Initial gain is 800).

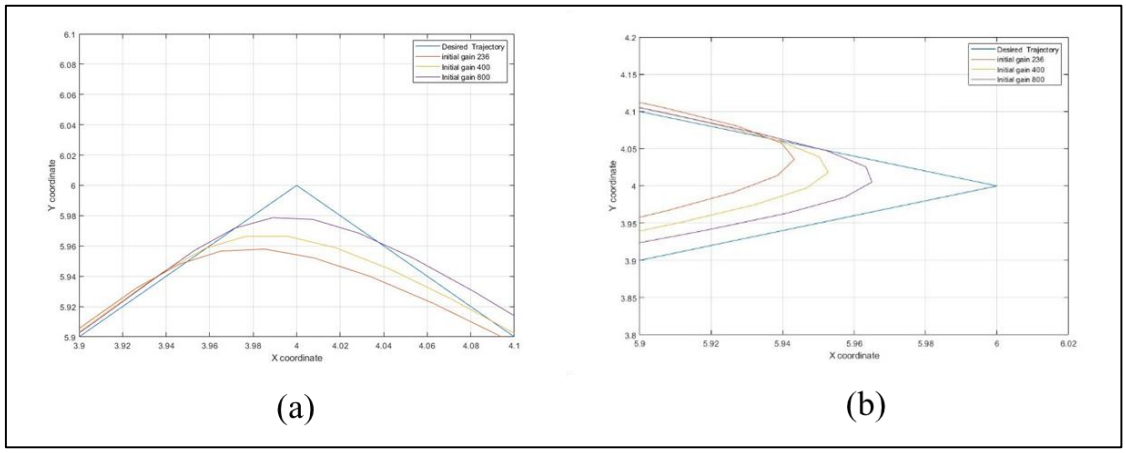

Figure 5. 14: System response of sharp corner tracking for different ILC gains (a) top corner and (b) right corner.

5.4 Contour Errors

The contour error is defined as error component orthogonal to the desired trajectory as previously mentioned. Fig. 5.15 and 5.16 shows the contouring error for model in Fig. 5.10 for different ILC gain values. As seen in Fig. 5.15 and 5.16, it is evident that at the sharp corner there is still some contour error albeit very small. It can be observed that the contouring error reduces with each iteration by implementing the Iterative Learning Control scheme proposed in this study.

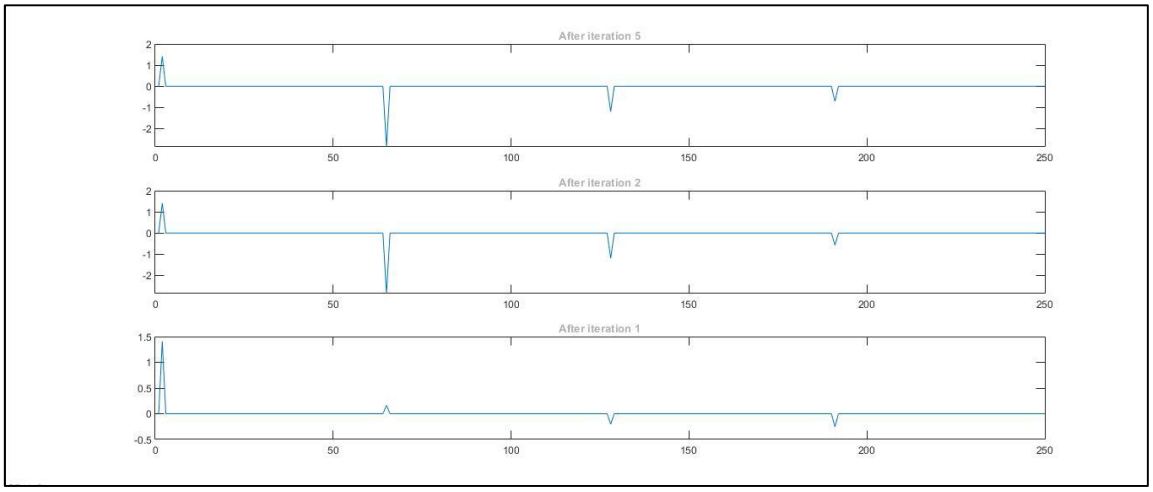

Figure 5. 15: Contour error obtained after several iteration for ILC with feedback compensation (case2 for model in Fig 5.8) .

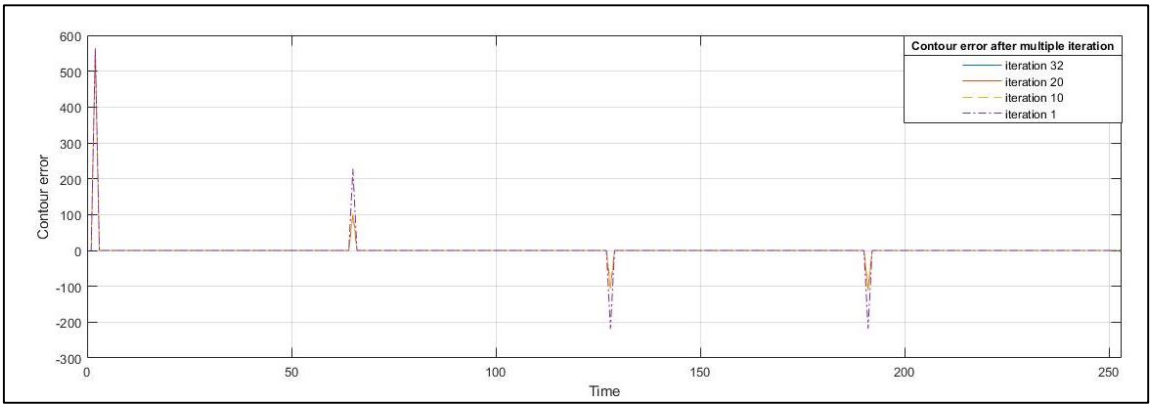

Figure 5. 16: Contour error obtained after several iterations (Initial gain = 400)

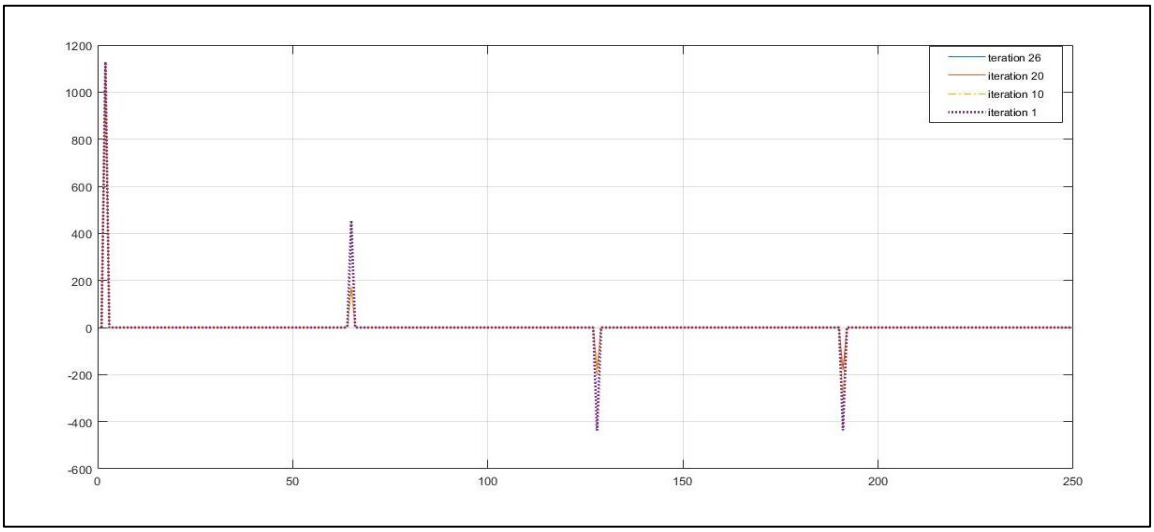

Figure 5. 17: Contour error obtained after several iterations (initial gain= 800).

Chapter 6

CONCLUSIONS

Additive manufacturing processes have a wide variety of parameters depending on the motion system utilized and process basic working principles. In this study, we focused on Fused Filament Fabrication (FFF) and Laser Metal Deposition (LMD) processes to understand and achieve better control strategies that can be implemented in AM systems. Three subsystems were discussed in Chapter 2 that include an XY positioning system, a liquefier system and a filament drive mechanism of a 3D printing system based on FFF technology.

The transfer functions for the liquefier block are obtained using system identification method as demonstrated in Chapter 2. Using the transfer functions identified we can design a suitable compensator to fulfill the desired outcome. The compensator designed in Section 2.1.7 reduced the settling time and steady state error. The temperature control system simulated also accounts for the filament feed rate (as a load to the system). For finer tuning of the system, the filament feed rate can be varied to achieve desired extruded filament shape (a size smaller than nozzle diameter).

An XY servomechanism-based positioning system is used in many additive manufacturing processes. The position system dynamics depends on its construction and inertia of the components. The finer control of this system is restricted by the driving capacity of servo motor driving the individual axis. The transfer function used in Chapter 5 is for a typical machine tool with XY servomechanism. Several control strategies were simulated in MATLAB Simulink for this system. The feedback compensation designed using Control

System Designer app of MATLAB was unable to produce favorable results. The iterative learning control (ILC) algorithm which was proven to be helpful in previous research on machine tool controls was then used to obtain satisfactory result. The reference trajectory used for simulation has four sharp corners which where quite difficult to follow as a motion path/trajectory for the system. Using the ILC algorithm for different values of gain and learning gain, the simulation results show that we were able to reduce the contour error. The ILC algorithm shows promising results to achieve the desired/reference trajectory. The ILC algorithm for different reference trajectory has to be adjusted individually by changing the gain values. Also, the number of iterations depend upon the reference trajectory coordinate and gain values. The ILC algorithm does not provide online control, hence it is useful when we have deterministic repeating disturbances and/or position errors.

The process control in Additive Manufacturing needs more future work especially in servomechanism, stepper motor systems type hardware implementations. The XY positioning system can be further coupled with liquefier and filament drive mechanisms or metal deposition mechanisms. It can be observed in Fig. 5.14 that after the sharp corner, the slope of x axis is more than the one in y axis. Therefore, if we slowed down the velocity of the x axis before we approach to a sharp corner we might be able to achieve even a better response. Future work in this field is required to achieve highly accurate and fast position and motion control systems.

BIBLIOGRAPHY

Arisoy, Y.M., Criales, L.E., Özel, T. (2019) Modeling and simulation of thermal field and solidification in laser powder bed fusion of nickel alloy IN625, Optics and Laser Technology, 109: 278–292.

Arisoy, Y.M., Criales, L.E., Özel, T., Lane, B., Moylan, S., Donmez, A. (2017) Influence of Scan Strategy and Process Parameters on Microstructure and Its Optimization in Additively Manufactured Nickel Alloy 625 via Laser Powder Bed Fusion," International Journal of Advanced Manufacturing Technology, 90 (5): 1393–1417.

Bourell, D.L., Rosen, D.W., Leu, M.C. (2014) The roadmap for additive manufacturing and its impact, 3D Print. Additive Manufacturing 1 (1): 6–9.

Chris T. F., Eric R., Jane H. B., Ann-Marie H., Katie L. M., Iterative Learning Control for Electrical Stimulation and Stroke Rehabilitation. Springer Briefs in Control, Automation and Robotics .ISBN 978-1-4471-6725-9. Pg 5-13

Chua C.H., Leong, K.F. (2015) 3D printing and additive manufacturing: principles and applications, World Scientific.

Costa, S.F., Duarte, F.M., Covas, J.A. (2017) Estimation of filament temperature and adhesion development in fused deposition techniques. Journal of Materials Processing Technology Vol. 245 pp. 167–179.

Criales L.E., Arisoy Y.M., Lane, B., Moylan, S., Donmez, A., Özel, T. (2017) Laser Powder Bed Fusion of Nickel Alloy 625: Experimental Investigations of Effects of Process Parameters on Melt Pool Size and Shape with Spatter Analysis. International Journal of Machine Tools and Manufacture.

Criales, L.E., Arisoy, Y.M., Özel, T. (2016) Sensitivity Analysis of Material and Process Parameters in Finite Element Modeling of Selective Laser Melting of Inconel 625. International Journal of Advanced Manufacturing Technology 86: 2653–2666.

Ertay, D.S., Yuen, A., Altintas, Y. (2017) Synchronized material deposition rate control with path velocity on fused filament fabrication machines. Additive Manufacturing 19 (2018) 205–213.

Domingo-Espin, M., Borros, S., Agullo, N., Garcia – Granada, A.A., Reyes, G. (2014) Influence of Building Parameters on the Dynamic Mechanical Properties of Polycarbonate Fused Deposition Modeling Parts. 3D Printing, Vol. 1 No. 2, doi:10.1089/3dp.2013.0007

Donadella S., Motta M., Demir A.G., Previtali B. (2018) Monitoring of laser metal deposition height by means of coaxial laser triangulation. Optics and laser in engineering 112 (2019) 136-144

Hassler U., Gruber D., Hentsschel O., Sukowski F., Grulich T., Seifert L. (2016) In-situ monitoring and defect detection for laser metal deposition by using infrared thermography. Physics Procedia 83:1244- 1252

Hagqvist P., Heralic A., Christiansson A. K., Lennartson B. (2015) Resistance based iterative learning control of additive manufacturing with wire. Mechatronics 31 (2015) 116-123

Heralic A., Christiansson A. K., Lennartson B., (2012) Height control of laser metal-wire deposition based on iterative learning control and 3D scanning. Optics and Lasers in Engineering 50: 1230-1241.

Hofman J.T., Pathiraj B., J. van Dijk, D.F. de Langec, Meijer J. (2012) A camera based feedback control strategy for the laser cladding process. Journal of Materials Processing Technology 212 (2012) 2455– 2462

Jason F., Lopez F.; Lane B., Yeung H., Grantham, Steven. (2016) On the requirements for model-based thermal control of melt pool geometry in Laser Powder Bed Fusion additive manufacturing. Materials Science and Technology 2016 (MS&T16)

Jerez-Mesa, R., Gomez, G., Travieso-Rodríguez, X., Corbella, R. Busque (2016) Finite element analysis of the thermal behavior of RepRap 3D printer liquefier. Mechatronics 36, pp.119-126

Kamath, C. (2016) Data mining and statistical inference in selective laser melting. The International Journal of Advanced Manufacturing Technology. 85(5): 1659–1677

Kamath, C., El-dasher B., Gallegos, G.F., Kinw, W.E., Sisto, A. (2014) Density of Additively-Manufactured, 316L SS Parts Using Laser Powder-Bed Fusion at Powers Up to 400W. The International Journal of Advanced Manufacturing Technology. 74:65-78.

Kempen, K., Thijs, L., Yasa, E., Badrossamay, M., Verheecke, M., Kruth, J.-P. (2011) Process Optimization and Microstructural Analysis for Selective Laser Melting of AlSi10Mg. Physics Procedia. 39: 439-446.

Krauss, H., Zeugner, T., Zaeh, M.F. (2014) Layerwise Monitoring of the Selective Laser Melting Process by Thermography. Physics Procedia 56: 64-71.

Lopez, F., Witherell, P., Lane, B. (2016) Identifying Uncertainty in Laser Powder Bed Fusion Additive Manufacturing Models. Journal of Mechanical Design. 138(11): 114502-1-4.

Mahesh, M., Lane, B., Donmez, A., Feng, S., Moylan, S., Fesperman, R. (2015) Measurement science needs for real-time control of additive manufacturing powder bed fusion processes. NIST Interagency/Internal Report (NISTIR) dx.doi.org/10.6028/NIST.IR.8036.

Mani, M., Lane, B., Donmez, A., Feng, S., Moylan, S., and Fesperman, R. (2015) Measurement Science Needs for Real-Time Control of Additive Manufacturing Powder Bed Fusion Processes. National Institute of Standards and Technology, Gaithersburg, MD, Standard No. NISTIR 8036.

Mertens, R., Clijsters, S., Kempen, K., Kruth, J-P. (2014) Optimization of Scan Strategies in Selective Laser Melting of Aluminum Parts With Downfacing Areas. Journal of Manufacturing Science and Engineering. 136(6): 061012-1-7.

Montgomery, C., Beuth, J., Sheridan, L., and Klingbeil, N. (2015) Process Mapping of Inconel 625 in Laser Powder Bed Additive Manufacturing. Solid Freeform Fabrication Symposium, pp. 1195–1204.

O'Regan, P., Prickett, P., Setchi, R., Hankins, G., Jones, N. (2016) Metal Based Additive Layer Manufacturing: Variations, Correlations and Process Control. Proceedings of the 20th International Conference on Knowledge-Based and Intelligent Information & Engineering Systems KES-2016. September 5-7, York, UK, 96: 216-224.

Özel, T., Criales, L.E., Arısoy, Y.M. (2016) Computational Simulation of Thermal and Spattering Phenomena and Microstructure in Selective Laser Melting of Inconel 625, Physics Procedia, 83:1435–1443.

Özel, T. Shaurya, A., Altay, A., Yang, L. (2018a) Process monitoring of meltpool and spatter for temporal-spatial modeling of laser powder bed fusion process, Procedia CIRP, 2018, 102–106. 10th CIRP Conference on Photonic Technologies, September 3-5, 2018, Fürth, Germany.

Özel, T., Altay, A., Donmez, A., Leach, R. (2018b) Surface topography investigations on nickel alloy 625 fabricated via laser powder bed fusion, International Journal of Advanced Manufacturing Technology, 94 (9–12): 4451–4458.

Pollard, D., Ward, C., Herrmann, G., Etches, J. (2017) Filament temperature dynamics in fused deposition modelling and outlook for control. Procedia Manufacturing 11: 536 – 544.

Shi, Q., Gu, D., Xi, M., Cao, S., Rong, T. (2016) Effects of laser processing parameters on thermal behavior and melting/solidification mechanism during selective laser melting of TiC/Inconel 718 composites, Optics & Laser Technology, 84: 9-22.

Shah, C.H., Shah, H.N., Patel, K., Özel, T. (2018) Effects of Liquefier Design On Thermal Profile in Fused Filament Fabrication Based Additive Manufacturing Process. The 18th International Conference on Machine Design and Production, July 3 – July 6 2018, Eskişehir, Turkey.

Srinivasan, K., Kulkarni, P.K. (1990) Cross-coupled control of biaxial feed drive servomechanisms. Journal of Dynamics Systems, Measurement, and Control, 112: 225-232.

Turner, B.N., Strong, R., Gold, S.A. (2014) A review of melt extrusion additive manufacturing processes: I. Process design and modelling. Rapid Prototyping Journal, Vol. 20 Issue: 3, pp.192-204.

Frazier, W.E. (2014) Metal Additive Manufacturing: A Review, Journal of Materials Engineering and Performance, 23:1917-1928

Yan, Z., Liu, W., Tang, Z., Liu, X., Zhang, N., Li M., Zhang, H., (2018) Review on thermal analysis in laser based Additive manufacturing. Optics and laser in engineering 106 (2018) 427-441

Zhang, B., Ziegert, J., Farahi, F., Davies, A. (2016) In situ surface topography of laser powder bed fusion using fringe projection. Additive Manufacturing 12: 100-1007.

Zhongwei, L., Xingjian, L., Shifeng, W., Piyao, H., Kai, Z., Qingsong, W., Yusheng, S., Sheng, L., (2018) In situ 3D monitoring of geometric signatures in the powder based fusion additive manufacturing process via vision sensing methods. Sensors 2018, 18,1180.